DESIGN MODIFICATION OF A FRONT WINDOW MECHANISM FOR THE CABIN OF AN EARTH MOVING MACHINE

A Thesis Submitted to
the Graduate School of Engineering and Sciences of
İzmir Institute of Technology
in Partial Fulfillment of the Requirements for the Degree of

MASTER OF SCIENCE

in Mechanical Engineering

by
Radomir JOVICHIKJ

July 2017
İZMİR

We approve the thesis of **Radomir JOVICHIKJ**

Examining Committee Members:

_____
Assoc. Prof. Dr. Gökhan KİPER
Department of Mechanical Engineering, İzmir Institute of Technology

_____
Assoc. Prof. Dr. Mehmet İsmet Can DEDE
Department of Mechanical Engineering, İzmir Institute of Technology

_____
Assist. Prof. Dr. Fatih Cemal CAN
Department of Mechatronics Engineering, İzmir Katip Çelebi University

31 July 2017

_____
Assoc. Prof. Dr. Gökhan KİPER
Supervisor
Department of Mechanical Engineering
İzmir Institute of Technology

_____
Prof. Dr. Metin TANOĞLU
Head of the Department of
Mechanical Engineering

_____
Prof. Dr. Aysun SOFUOĞLU
Dean of the Graduate School of
Engineering and Sciences

ACKNOWLEDGEMENTS

I would love to express my sincere gratitude to my family, especially my father for giving me the greatest motivation and support to have this thesis done.

I would also like to thank to my supervisor Dr. Gökhan Kiper, and my respected professors Dr. M. İ. Can Dede and Dr. Seçil Artem for their guidance during my M.Sc. studies in İzmir Institute of Technology.

I would like to express my deepest appreciation to all my lab mates, Mr. Tetik, Mr. Eraz, Mr. Karagöz, Mr. Demirel, Miss. Özkahya, for their companionship, hospitality and help for this thesis study.

ABSTRACT

DESIGN MODIFICATIONS OF A FRONT WINDOW MECHANISM FOR THE CABIN OF AN EARTH MOVING MACHINERY

This thesis study investigates the front window mechanism used in an earth moving machinery. Since the mechanism is actuated by the operator, the required actuation force for the mechanism needs to be as minimum as possible. The problem of this thesis is defined by Turkey branch of Mecalac Company and the final test of this study are performed in their facility.

First, the problem definition and aim of the study is presented. Furthermore, the literature review is also presented. Then, the current mechanism attached on the earth moving machinery is investigated. Firstly, kinematic analysis is performed in order to be able to perform the force analysis. Following that, using three different approaches (Newton-Euler approach, virtual work method and graphical approach), the static force analysis is done. The aim of this analysis to obtain the required actuation force, both for opening and closing the mechanism. By using three different approaches, the result obtained after each method are compared and confirmed. Furthermore, a simulation of the mechanism is prepared in MATLAB/Simulink® environment. This step provided a numerical simulation verification for the resulting actuation forces. Then the work carried out for the minimization of the actuation force is presented. By changing the parameters of the springs attached on the current mechanism, changing the link lengths of the mechanism and changing the application point of the actuation force, the change in the magnitude of the required actuation force is observed and minimized. Among all trials, only changing the spring position led to useful results. Finally, the test setup to measure the performance and experimentally verify the proposed solution is explained and the results are given. The results show that with the modified location of the spring, both of the maximum force requirements and the work requirements are lowered.

ÖZET

BİR İŞ MAKİNASI KABİNİ İÇİN ÖN CAM MEKANİZMASI TASARIM GÜNCELLEMESİ

Bu tez çalışması bir iş makinasında kullanılan ön camı tahrik eden bir mekanizmayı incelemektedir. Bahsi geçen ön camı operator tarafından el ile tahrik edildiğinden, gerekli olan tahrik kuvveti olabildiğince az olmalıdır. Bu tez çalışmasına konu olan problem, Mecalac şirketinin Türkiye ofisi tarafından tanımlanmıştır ve çalışmanın değerlendirilmesi için gerekli testler bahsi geçen firmada yapılmıştır.

Önce problem tanımı ve tez çalışmasının amacı verilmiştir. Ayrıca, yapılmış olan literatür araştırması da sunulmuştur. Sonra, iş makinası üzerinde aktif olarak kullanılan mekanizma incelenmiştir. Mekanizmanın kinematik analizi ile static kuvvet analizleri sunulmuştur. Statik kuvvet analizi üç farklı yöntem (Newton-Euler metodu, virtüel iş pirensibi ve grafik yöntem) kullanılarak yapılmıştır. Bu analizlerin amacı, mekanizmayı açmak ve kapatmak için gerekli olan tahrik kuvvetlerinin hesaplanmasıdır. Üç farklı yöntem kullanılarak, elde edilen sonuçlar karşılaştırılmış ve doğrulanmıştır. Ayrıca, MATLAB/Simulink® ortamında hazırlanmış olan bir simülasyon da sunulmuştur. Böylece statik kuvvet analizi sonucunda elde edilen değerler bir simülasyon tarafından doğrulanmıştır. Daha sonra mekanizmada mevcut bulunan yay, uzuv boyutları, tahrik kuvveti uygulama noktası gibi parametreler değiştirilerek, mekanizmayı tahrik etmek için gerekli olan kuvvet azaltılmaya çalışılmıştır. Tüm bu denemelerden yalnızca yayın yerinin değiştirilmesi faydalı sonuç vermiştir. Son olarak, tahrik kuvvetinin minimize edilmesi için önerilen yöntemin doğrulanması amacıyla tasarlanmış test düzeneği ve elde edilen sonuçlar verilmiştir. Elde edilen sonuçlara göre yeni yay konumunda hem azami kuvvet gereksinimi, hem de toplam yapılan işte azalma olduğu tespit edilmiştir.

TABLE OF CONTENTS

LIST OF FIGURES

Figure **Page**

LIST OF TABLES

Table **Page**

CHAPTER 1

INTRODUCTION

An earth moving machinery is self-propelled or towed machine on wheels, crawlers or legs, having equipment or attachment (working tool), or both, primarily designed to perform excavation, loading, transportation, drilling, spreading, compacting or trenching of earth, rock and other materials. It consists of the following types of machine groups: dozers, loaders, backhoe loaders, excavators, trenches, dumpers, scrapers, graders, landfill compactors, rollers, pipelayers, horizontal directional drills and compact tool carriers (ISO 10261:2002 Definition).

Earth moving machines comprise many application-specific mechanisms, some of which are related with the operation and some of which are related with the necessities of the operator. This thesis deals with the front window mechanism of a small scale excavator, namely the 6MCR Crawler Skid-Excavator (Figure 1.1) of Mecalac company manufactured in the Aegean Free Zone in İzmir. The machine is known for its compactness, fuel efficiency, versatility in the sense of multipurpose usage as excavator and loader and shows high performance in terms of high load capacity with respect to its size speed and agility (Mecalac, 'MCR Mecalac').

In the following subsections of this Chapter, the problem definition, the aim of the study and the literature review is given. Chapter 2 consists of the analysis of the existing mechanism, where kinematic and static force analysis were performed. Chapter 3 presents solution alternatives such as spring position variation, link length and handle position optimization and their results. In Chapter 4 one of the solution alternatives is implemented on a cabin and tests are conducted to verify if the proposed solution enhances the design. Chapter 5 comprises discussion on the results and the conclusions.

Figure 1.1. 6MCR Crawler Skid-Excavator
(Source: http://www.mecalac.com/en/machine/6mcr.html)

1.1 Problem Definition and Aim of the Thesis

The problem that is studied in the thesis has been defined by the Turkey branch of the Mecalac company. As they got feedback from the operators using the excavators, the window opening mechanism shown in Figure 1.2 needs to be redesigned which is the motivation for this thesis. The main problem is the force requirement for opening and closing the window. Furthermore, the operators that have an average height around 170 to 180 cm have no ergonomic problem operating the current mechanism, but the operators below average height are having trouble while reaching the handles to open the window and drive the mechanism. For the operators above average height the problem arises with the limitation of the workspace. While the window is being opened they need to lean down during the action. To solve these problems, revision of the design is needed.

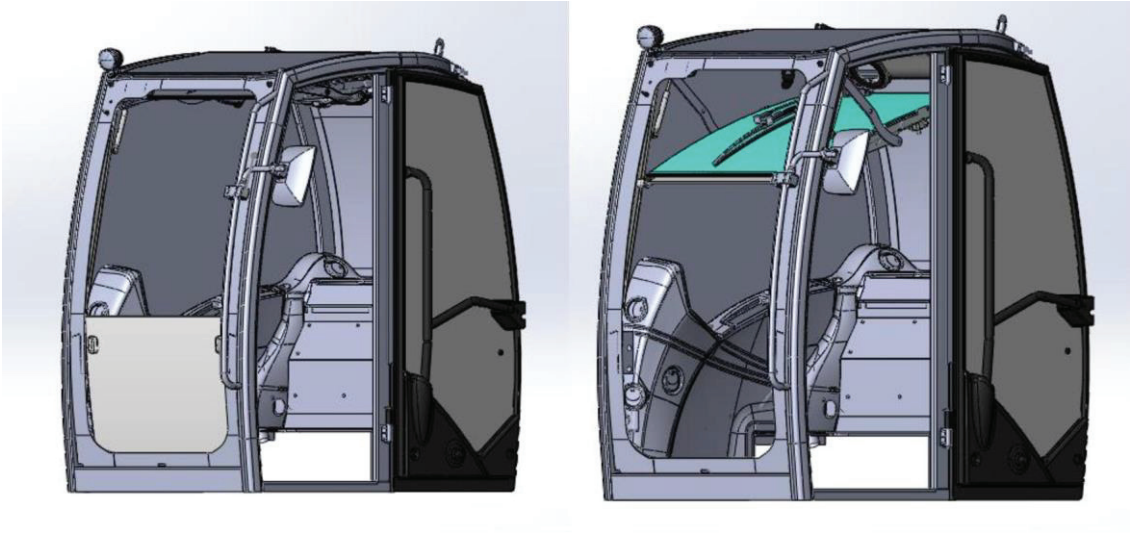

Figure 1.2. Cad Model of the Two Configurations of the Mechanism: a) Without the Lower Window, b) With the Lower Window

The front window has two parts: a lower window and an upper window. A complication of the problem is that the mechanism has a second degree of freedom which allows to attach the lower window to the upper window which changes the weight to be carried and limits of the workspace of the system. Figure 1.2a illustrates the case where only the upper window is open, while Figure 1.2b illustrates the case where the lower window is attached to the inner side of the upper window and the window is open.

The aim of the thesis is to seek the necessary modifications for the mechanism design in order to minimize the force requirements of the system. For the design of the mechanism there are some constraints like the shape of the cabin, that the window cannot be changed, and the design has to be simple and easy to produce.

1.2 Literature Review

There are no scientific papers, or books about this problem, so the literature review consists of the patents for window opening mechanisms of construction machinery.

Since the purpose of the thesis was to enhance the mechanism design, patents were investigated in order not to have similar designs which are patented.

One of the patents uses a cable driven double slider mechanism as shown in Figure 1.3. In the lower and upper part of the frame there is a roller attached which is slotted in the cabin frame. In the upper part of the cabin there is a geared guide for the cable. The cable is then connected to the lower rollers. When the cables are pulled by the motor the mechanism moves in the upper direction. When the motor releases the cable mechanism moves in the downwards direction under the effect of gravitational force.(Hiraoka et al. 1992)

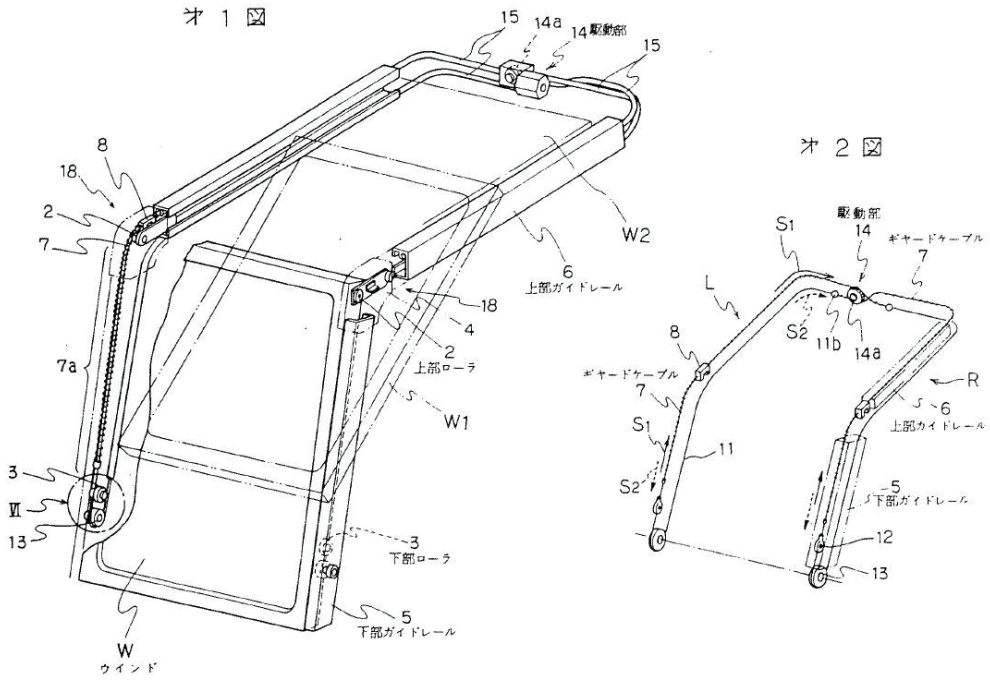

Figure 1.3. Schematics of Cable Driven Double Slider Mechanism
(Source: Hiraoka et al. 1992)

Another patented mechanism for window opening makes use of a wire retaining pin that moves in a guide rail. At one end the wire is connected to the spring and at the other end it is connected with a wire retaining pin as shown in Figure 1.4. In the closed configuration the tension of the wire acts on the front window as a pressing force and pushes the window forward, and when the front window is being opened the tension acts through the link on the front window as an assisting force (Fujii and Ookubo 2007).

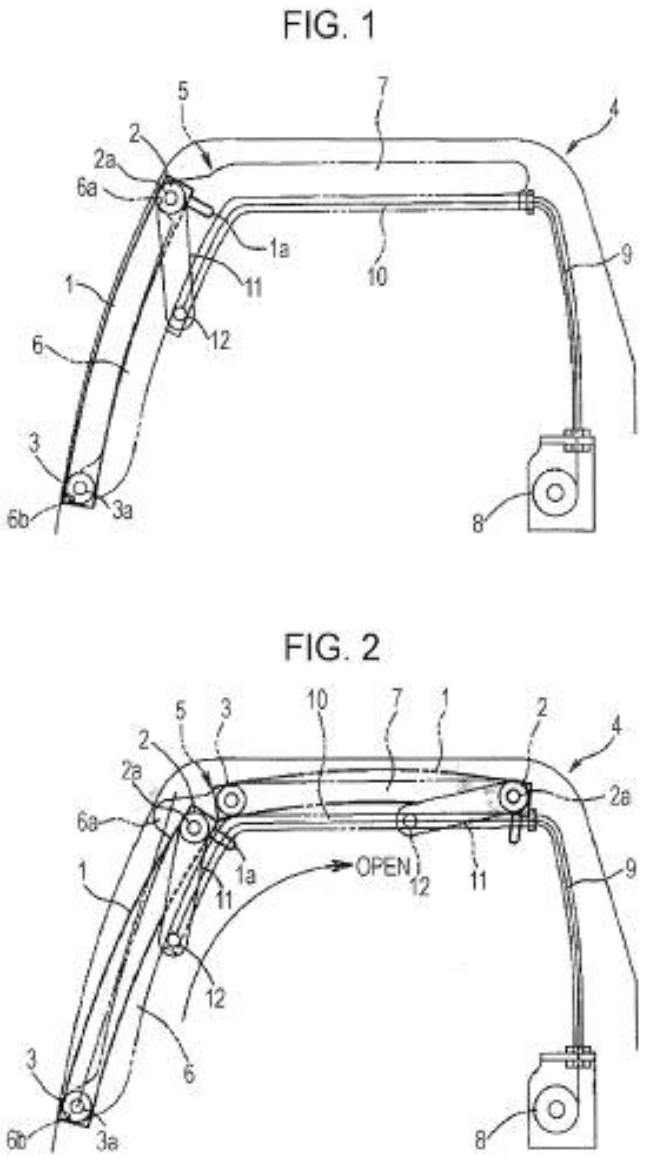

Figure 1.4. Open and Closed Configuration of Mechanism with Wire Retaining Pin (Source: Fujii and Ookubo 2007)

Another patent is about a mechanism which utilizes a restoring force of a spiral spring as an assisting force in opening and closing the mechanism. The mechanism has slotted rollers to obtain the motion. The assisting force lowers the overall force that the operator needs to use in order to open or close the mechanism. The mechanism is basically a double-slider mechanism as it can be seen in Figure 1.5 and it is operated manually by the operator (Kakegawa and Murakami 2009).

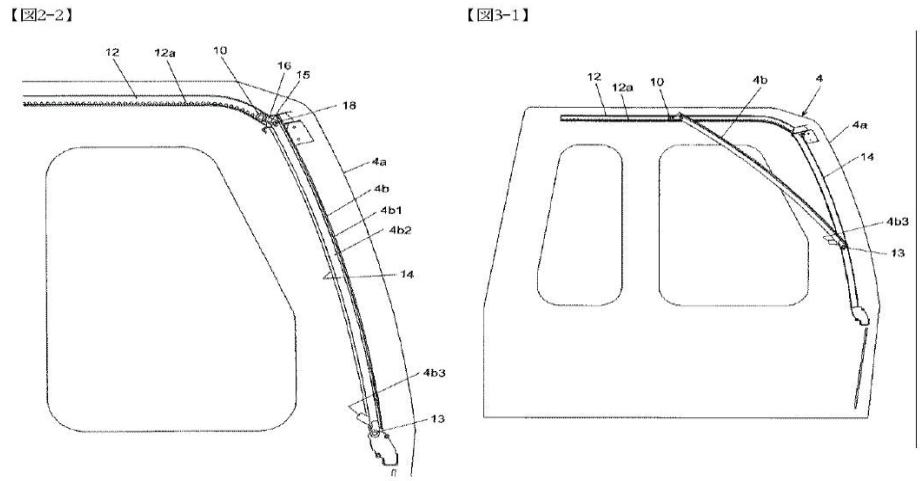

Figure 1.5. Open and Closed Configuration of Mechanism
(Source: Kakegawa and Murakami 2009)

The mechanism issued in the next patent is similar to the one in this thesis. It is composed of lower and upper windows. In closed form, there are two options: to open the upper window only or both of them all together. For the second case the lower window is detached from the cabin frame and attached to the rear side of the upper window with a locking mechanism as show in Figure 1.6. The upper window has roller guides in the lower and upper part of the window frame. The opening and closing operation is done by the operator manually. (Hayashida and Hirano 2013)

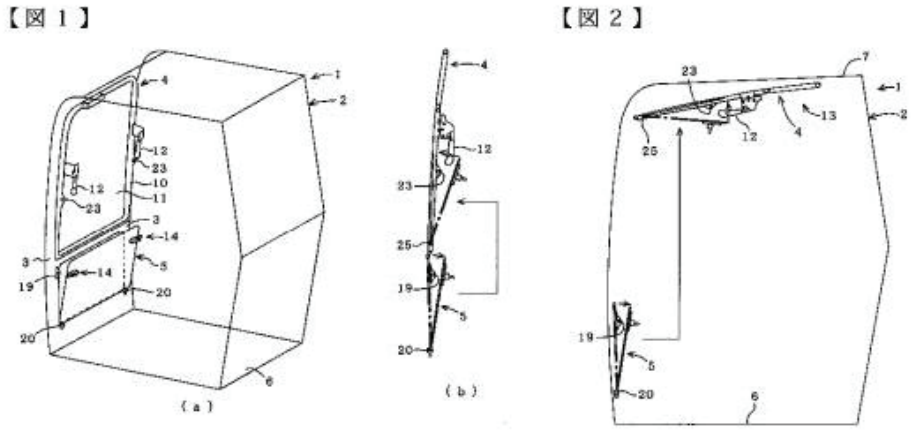

Figure 1.6. Schematics of the Two Possible Configurations of the Mechanism
(Source: Hayashida and Hirano 2013)

CHAPTER 2

EXISTING MECHANISM

The existing mechanism used to manipulate the front window is a planar slider crank mechanism (Figure 2.1). Link A_0A is the crank and link AB is the connecting rod (or coupler link), which is attached to the front window of the vehicle. To balance the window during the motion of the slider crank mechanism, a linear spring is attached between the base (the cabin) and the crank at points C and D respectively. Point E is considered as the point of application of the manual actuation force.

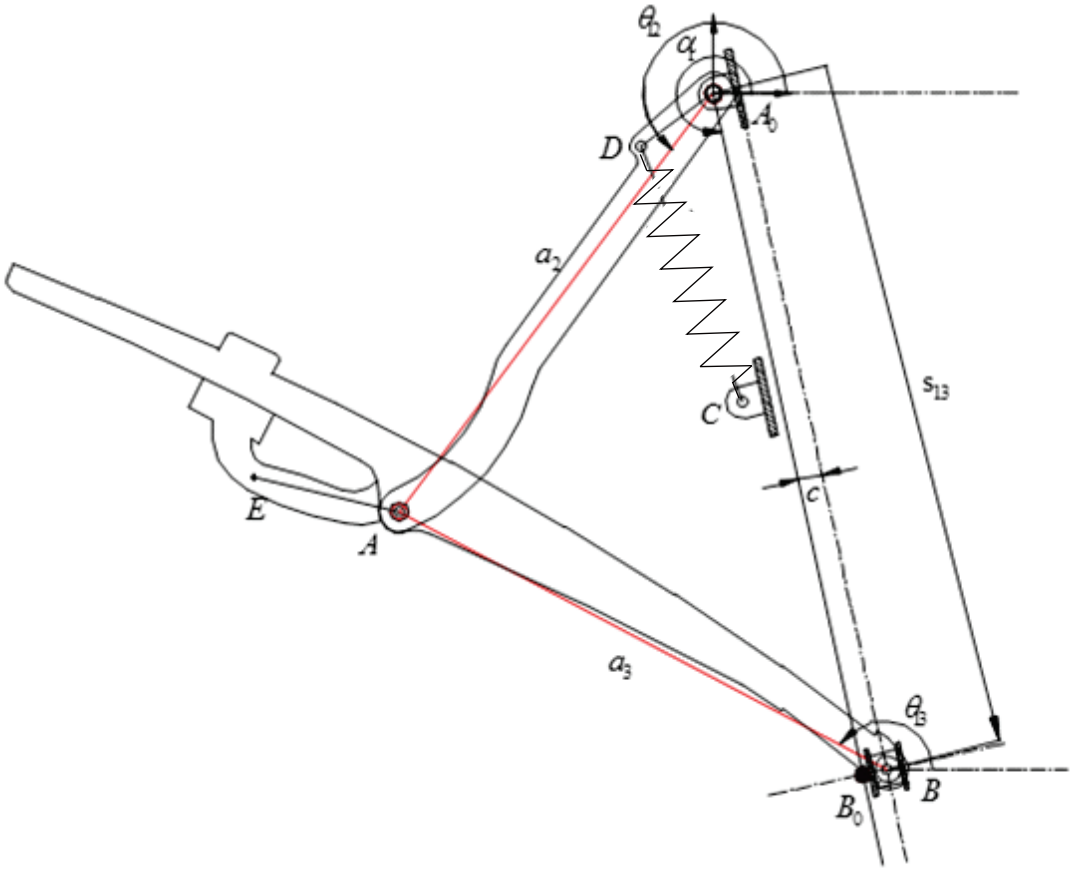

Figure 2.1. Kinematic Scheme of the Current Mechanism

The coordinate frame is attached at point A_0. The revolute joints of the slider-crank mechanism are at A_0, A and B. The prismatic joint (slider) variable is measured from the projection of A_0 to the line passing through B in the sliding direction. The slider-crank mechanism has the following structural dimensions: crank: a_2 = 440 mm, coupler: a_3 = 463.6 mm and eccentricity c = 6.6 mm. The sliding direction makes an angle of α_1 = 282.29° with the horizontal x-axis (assuming the gravity acts in $-y$ direction).

The motion is not so dynamic, therefore just the kinetostatic analysis of the mechanism is performed, i.e. the velocity and acceleration analyses as well as dynamic force or motion analysis are not performed.

2.1 Kinematics of the Mechanism

The input of the mechanism is chosen as θ_{12}. The loop closure equation for the mechanism can be written as:

$$\begin{aligned} \overrightarrow{A_0A} &= \overrightarrow{A_0B_0} + \overrightarrow{B_0B} + \overrightarrow{BA} \\ a_2 e^{i\theta_{12}} &= s_{13} e^{i\alpha_1} + c e^{i(\alpha_1+\pi/2)} + a_3 e^{i\theta_{13}} \end{aligned} \tag{2.1}$$

When the loop closure equation is separated into its x- and y-components and rearranged, θ_{13} can be eliminated from the equation:

$$\begin{aligned} &\left\{a_2\cos\theta_{12} - \mathrm{s}_{13}\cos\alpha_1 - c\sin\alpha_1 = a_3\cos\theta_{13}\right\}^2 \\ &+ \left\{a_2\sin\theta_{12} - \mathrm{s}_{13}\sin\alpha_1 - c\cos\alpha_1 = a_3\sin\theta_{13}\right\}^2 \\ &U\,\mathrm{s}_{13}^2 + V\,\mathrm{s}_{13} + W = 0 \end{aligned} \tag{2.2}$$

where

$$\begin{aligned} U &= 1 \\ V &= 2c\sin(2\alpha_1) - 2\cos(\alpha_1 - \theta_{12})a_2 \\ W &= c^2 - 2c\sin(\alpha_1 + \theta_{12})a_2 + a_2^2 - a_3^2 \end{aligned}$$

s_{13} can be solved from Equation (2.2):

$$\mathrm{s}_{13} = \frac{-V \pm \sqrt{V^2 - 4UW}}{2U} \tag{2.3}$$

When s_{13} is obtained from Equation (2.3), θ_{13} can be solved using Equation (2.1) :

$$\theta_{13} = \mathrm{atan2}\left[a_2\cos\theta_{12} - \mathrm{s}_{13}\cos\alpha_1 - c\sin\alpha_1, a_2\sin\theta_{12} - \mathrm{s}_{13}\sin\alpha_1 - c\cos\alpha_1\right] \tag{2.4}$$

2.2 Static Force Analysis

For the static force analysis three different approaches are used in order to be able to obtain the required handling force and compare the results. The first method used is based on Newton's equilibrium equations. The second method is the virtual work method (VWM), which is an energy based approach. The last method is the graphical approach which is used in order to confirm the results obtained from the other two methods. In this method, a static force analysis is performed for the mechanism in a certain configuration.

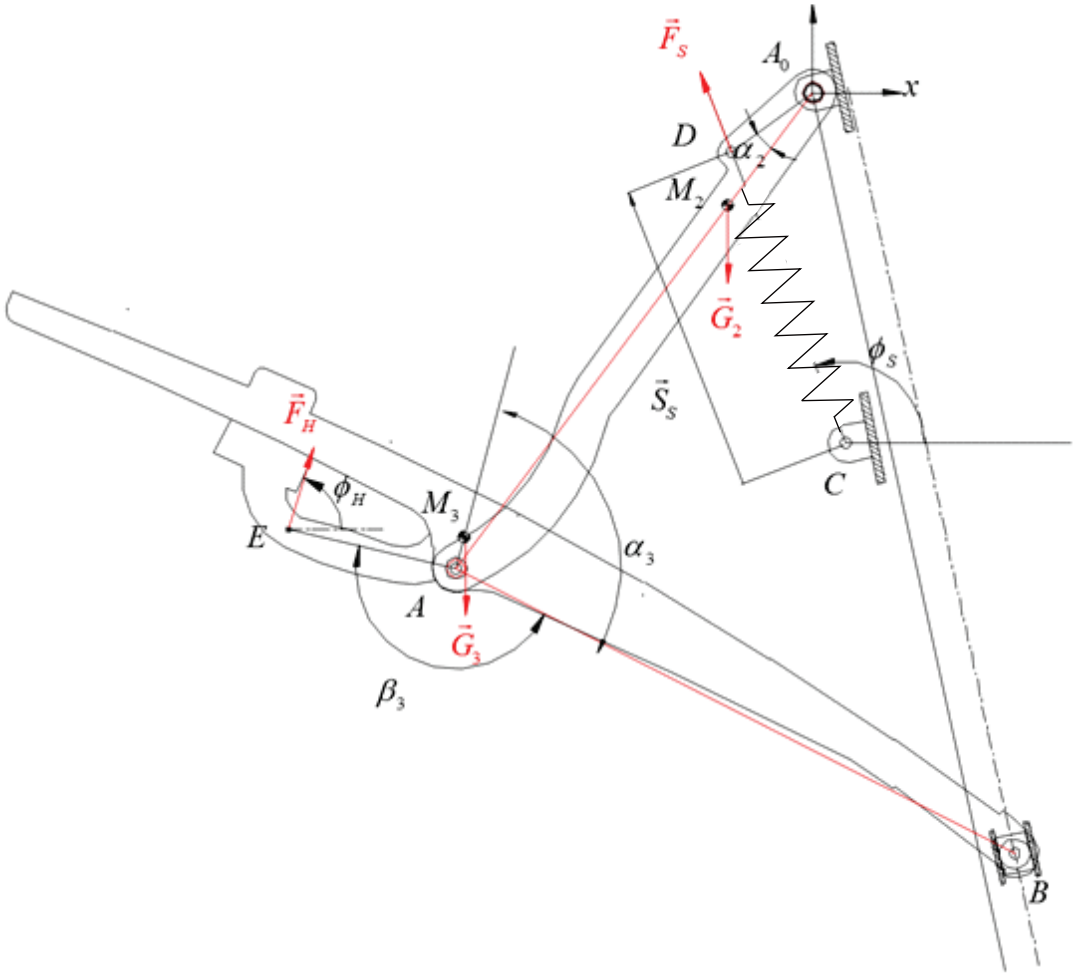

Figure 2.2. External Forces Acting on the Mechanism

As presented in Figure 2.2, there are four external forces applied on the system: the weights of the crank and the coupler, $\vec{G}_2$ and $\vec{G}_3$, the spring force, $\vec{F}_S$, and the

actuation force, $\vec{F}_H$. The mass of link 2 is $m_2 = 3.83$ kg. The mass of link 3 differs whether the lower window is attached to the mechanism ($m_3 = 21.7$ kg) or not ($m_3 = 16.18$ kg).

For the static force analysis three different approaches are used in order to be able to obtain the required handling force and compare the results. The first method used is based on Newton's equilibrium equations. The second method is the virtual work method (VWM), which is an energy based approach. The last method is the graphical approach which is used in order to confirm the results obtained from the other two methods. In this method, a static force analysis is performed for the mechanism in a certain configuration.

The center of mass of link 2 lies on point M_2. $|A_0M_2|$ distance is given as $l_2 =$ 104.6 mm. The center of mass of link 3 is shown with M_3. $|AM_3|$ distance is called as l_3 and $\angle BAM_3$ angle is defined as α_3. Without the lower window $l_3 = 20.94$ mm and $\alpha_3 =$ 93.09° . If the lower window is attached $l_3 = 48.79$ mm and $\alpha_3 = 24.69°$.

The linear gas springs that are used in the mechanism are of the type Stabilus Lift-O-Mat 083380 0500N and the characteristics of the force are given in Figure 2.3.

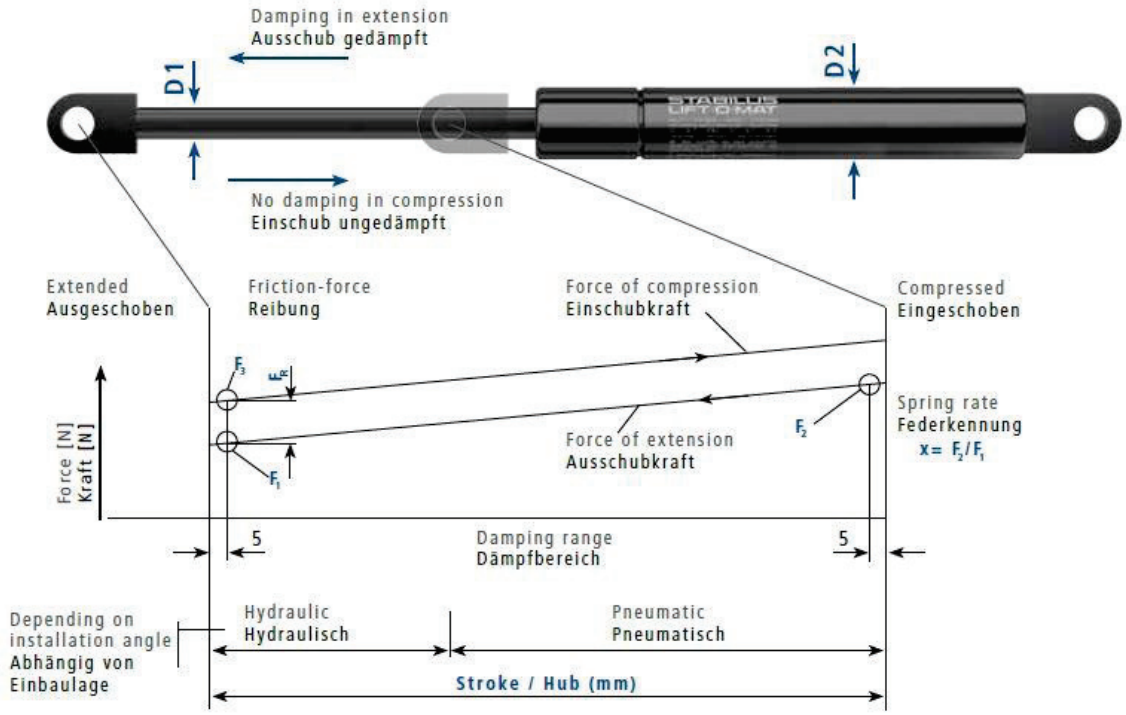

Figure 2.3. Force Characteristics of the Spring

The force that the spring supplies at the fully extended position is $F_{S_1} = 500\text{N}$. The spring rate coefficient is given as x = 1.35. This spring rate coefficient is used to calculate $F_{S_2} = xF_{S_1} = 675\text{N}$, which is the force that the spring supplies at the fully compressed position. The maximum length of the spring is $S_{S_{\max}} = 285$ mm and the minimum length is $S_{S_{\min}} = 185$ mm. The linear spring is attached to the system at points C and D. Point C is fixed and its coordinates are measured as $\overrightarrow{A_0C} = \begin{bmatrix} C_x & C_y \end{bmatrix} = \begin{bmatrix} 23.62 & -257.13 \end{bmatrix}$ mm with respect to the coordinate frame given in Figure2-3.

The position of point D is calculated as:

$$\overrightarrow{A_0D} = \begin{bmatrix} D_x & D_y \end{bmatrix} = b_2 e^{i(\theta_{12} - \alpha_2)} \tag{2.5}$$

At any instant, the length of the spring is calculated as:

$$S_S = \sqrt{\left(D_x - C_x\right)^2 + \left(D_y - C_y\right)^2} \tag{2.6}$$

The force that is required by (F_{SC}) or obtained from (F_{SO}) the spring are calculated as:

$$F_{SO} = 2\left(F_{S_2} - \frac{F_{S_2} - F_{S_1}}{S_{S_{\max}} - S_{S_{\min}}}\left(S_S - S_{S_{\min}}\right) \right) \tag{2.7}$$

$$F_{SC} = 2\left(F_{S_2} + F_{S_3} - \frac{F_{S_2} - F_{S_1}}{S_{S_{\max}} - S_{S_{\min}}}\left(S_S - S_{S_{\min}}\right) \right) \tag{2.8}$$

where $F_{S_3} = 60$ N is the friction force that occurs during the compression of the spring. All the numerical values and formulations are obtained by the information given in (Stabilus.com, "Gas Springs and Dampers for Industrial Applications").

The main problem is to obtain the required actuation force. The actuation force is shown with $\vec{F}_H$ and the point of application of this force is an arbitrarily selected point on the handle (point E). The position of point E is calculated as:

$$\overrightarrow{A_0E} = \overrightarrow{A_0A} + \overrightarrow{AE} = a_2 e^{i\theta_{12}} + b_3 e^{i(\theta_{13} + \pi + \beta_3)} \tag{2.9}$$

where $b_3 = \left|AE\right| = 100$ mm and $\beta_3 = \angle BAE = 162.75°$. The orientation of the actuation force, ϕ_H, is assumed to be always collinear with the velocity vector of point E. The

direction of the velocity vector at point E is calculated by differentiating Equation (2.9) with respect to θ_{12} as:

$$\phi_H = a_2 e^{-i\theta_{12}} + b_3 \frac{d\theta_{13}}{d\theta_{12}} e^{-i(\theta_{13}+\pi+\beta_3)} \tag{2.10}$$

2.2.1 Static Force Analysis with Newton-Euler Approach

To perform the static force analysis using Newton-Euler approach, the free-body-diagrams (FBD) of the links are drawn and the force/moment equilibrium conditions are written for each link. The static equilibrium conditions for the crank shown in Figure 2.4 are:

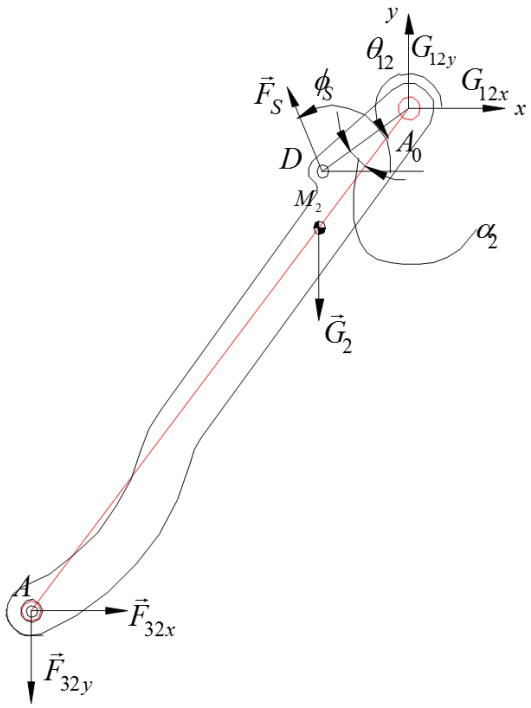

Figure 2.4. FBD of Link 2

$$\sum F_x = G_{12x} + F_{32x} + F_s \cos(\phi_s) = 0 \tag{2.11}$$

$$\sum F_y = G_{12y} - F_{32y} - G_2 + F_s \sin(\phi_s) = 0 \tag{2.12}$$

$$\sum M_{A_0} = \left\{ \begin{array}{c} a_2 F_{32y} \sin\left(-\pi/2 - \theta_{12}\right) + a_2 F_{32x} \sin\left(-\theta_{12}\right) \\ +G_2 l_2 \sin\left(-\pi/2 - \theta_{12}\right) + b_2 F_S \sin\left(\phi_S - \theta_{12} + \alpha_2\right) \end{array} \right\} = 0 \tag{2.13}$$

The equilibrium conditions for link 3 shown in Figure 2.5 are:

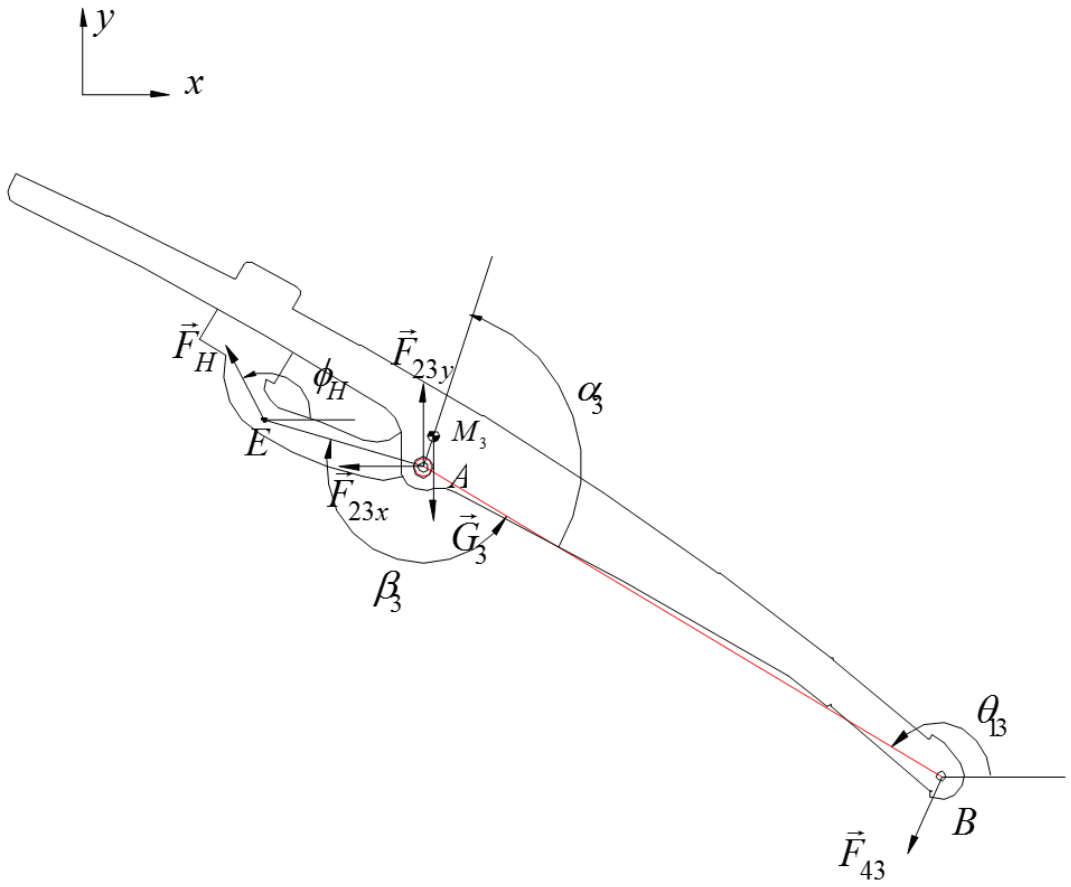

Figure 2.5. FBD of Link 3

$$\sum F^x = -F_{32x} - F_{43}\cos\left(\alpha_1 - \pi/2\right) + F_H\cos\left(\phi_H\right) = 0 \tag{2.14}$$

$$\sum F^y = F_{32y} - F_{43}\sin\left(\alpha_1 - \pi/2\right) - G_3 + F_H\sin\left(\phi_H\right) = 0 \tag{2.15}$$

$$\sum M_A = \left\{\begin{array}{c} a_3F_{43}\sin\left(\alpha_1 - \pi/2 - \theta_{13}\right) + l_3G_3\sin\left(-3\pi/2 - \theta_{13} - \alpha_3\right) + \\ b_3F_H\sin\left(\phi_H - \theta_{13} - \pi + \beta_3\right) \end{array}\right\} = 0 \tag{2.16}$$

By defining Equations (2.11)-(2.16), 6 equations in terms of 6 unknowns (G_{12x}, G_{12y}, F_{32x}, F_{32y}, F_{43} and F_H) are obtained. By linearly solving these equations, the unknown forces can be obtained as given in the following equations:

$$G_{12x}=\frac{\left\{a_2\left[\begin{array}{c} b_3\sin\left(\beta_3-\theta_{13}+\phi_H\right)\left[G_3\cos\theta_{12}\sin\alpha_1-F_S\cos\left(\alpha_1-\theta_{12}\right)\cos\phi_s\right] \\ +a_3\cos\left(\alpha_1-\theta_{13}\right)\left[G_3\cos\theta_{12}\cos\phi_s-F_S\cos\phi_s\sin\left(\theta_{12}-\phi_H\right)\right] \\ -G_3l_3\cos\theta_{12}\cos\left(\alpha_3+\theta_{13}\right)\cos\left(\alpha_1-\phi_H\right)\end{array}\right]-\left[\begin{array}{c} b_2F_S\sin\left(\alpha_2-\theta_{12}+\phi_s\right) \\ -G_2l_2\cos\theta_{12}\end{array}\right]\left[\begin{array}{c} b_3\sin\alpha_1\sin\left(\beta_3-\theta_{13}+\phi_H\right) \\ +a_3\cos\left(\alpha_1-\theta_{13}\right)\cos\phi_s\end{array}\right]\right\}}{a_2\left[\begin{array}{c} b_3\cos\left(\alpha_1-\theta_{12}\right)\sin\left(\beta_3-\theta_{13}+\phi_H\right) \\ +a_3\cos\left(\alpha_1-\theta_{13}\right)\sin\left(\theta_{12}-\phi_H\right)\end{array}\right]} \tag{2.17}$$

$$G_{12y}=\frac{\left\{a_2\left[\begin{array}{c} b_3\sin\left(\beta_3-\theta_{13}+\phi_H\right)\left[\cos\left(\alpha_1-\theta_{12}\right)\left(G_2-F_S\sin\phi_s\right)+G_3\sin\alpha_1\sin\theta_{12}\right] \\ +a_3\cos\left(\alpha_1-\theta_{13}\right)\left[\sin\left(\theta_{12}-\phi_H\right)\left(G_2-F_S\sin\phi_s\right)+G_3\cos\phi_H\sin\theta_{12}\right] \\ -G_3l_3\cos\left(\alpha_3+\theta_{13}\right)\cos\left(\alpha_1-\phi_H\right)\sin\theta_{12}\end{array}\right]-\left[\begin{array}{c} b_2F_S\sin\left(\alpha_2-\theta_{12}+\phi_s\right) \\ -G_2l_2\cos\theta_{12}\end{array}\right]\left[\begin{array}{c} b_3\cos\alpha_1\sin\left(\beta_3-\theta_{13}+\phi_H\right) \\ -a_3\cos\left(\alpha_1-\theta_{13}\right)\sin\phi_H\end{array}\right]\right\}}{a_2\left[\begin{array}{c} b_3\cos\left(\alpha_1-\theta_{12}\right)\sin\left(\beta_3-\theta_{13}+\phi_H\right) \\ +a_3\cos\left(\alpha_1-\theta_{13}\right)\sin\left(\theta_{12}-\phi_H\right)\end{array}\right]} \tag{2.18}$$

$$F_{32x}=\frac{\left\{\begin{array}{c} b_2F_S\sin\left(\alpha_2-\theta_{12}+\phi_s\right)\left[\begin{array}{c} b_3\sin\alpha_1\sin\left(\beta_3-\theta_{13}+\phi_H\right) \\ +a_3\cos\left(\alpha_1-\theta_{13}\right)\cos\phi_H\end{array}\right] \\ +\cos\theta_{12}\left[\begin{array}{c} -a_2b_3G_3\sin\alpha_1\sin\left(\beta_3-\theta_{13}+\phi_H\right) \\ -b_3G_2l_2\sin\alpha_1\sin\left(\beta_3-\theta_{13}+\phi_H\right) \\ +a_2G_3l_3\cos\left(\alpha_3+\theta_{13}\right)\cos\left(\alpha_1-\phi_H\right) \\ -a_3\left(a_2G_3+G_2l_2\right)\cos\left(\alpha_1-\theta_{13}\right)\cos\phi_H\end{array}\right]\end{array}\right\}}{a_2\left[\begin{array}{c} b_3\cos\left(\alpha_1-\theta_{12}\right)\sin\left(\beta_3-\theta_{13}+\phi_H\right) \\ +a_3\cos\left(\alpha_1-\theta_{13}\right)\sin\left(\theta_{12}-\phi_H\right)\end{array}\right]}. \tag{2.19}$$

$$F_{32y}=\frac{\left\{\begin{array}{c} a_2G_3\sin\theta_{12}\left[\begin{array}{c} b_3\sin\alpha_1\sin\left(\beta_3-\theta_{13}+\phi_H\right) \\ -l_3\cos\left(\alpha_3+\theta_{13}\right)\cos\left(\alpha_1-\phi_H\right) \\ +a_3\cos\left(\alpha_1-\theta_{13}\right)\cos\phi_H\end{array}\right] \\ +b_2F_S\sin\left(\alpha_2-\theta_{12}+\phi_s\right)\left[\begin{array}{c} b_3\cos\alpha_1\sin\left(\beta_3-\theta_{13}+\phi_H\right) \\ -a_3\cos\left(\alpha_1-\theta_{13}\right)\sin\phi_H\end{array}\right] \\ +G_2l_2\cos\theta_{12}\left[\begin{array}{c} -b_3\cos\alpha_1\sin\left(\beta_3-\theta_{13}+\phi_H\right) \\ +a_3\cos\left(\alpha_1-\theta_{13}\right)\sin\phi_H\end{array}\right]\end{array}\right\}}{a_2\left[b_3\cos\left(\alpha_1-\theta_{12}\right)\sin\left(\beta_3-\theta_{13}+\phi_H\right)+a_3\cos\left(\alpha_1-\theta_{13}\right)\sin\left(\theta_{12}-\phi_H\right)\right]} \tag{2.20}$$

$$F_{43}=\frac{\left\{\begin{array}{c} b_3\sin\left(\beta_3-\theta_{13}+\phi_H\right)\left[\left(a_2G_3+G_2l_2\right)\cos\theta_{12}-b_2F_S\sin\left(\alpha_2-\theta_{12}+\phi_s\right)\right] \\ +a_2G_3l_3\cos\left(\alpha_3+\theta_{13}\right)\sin\left(\theta_{12}-\phi_H\right) \end{array}\right\}}{a_2\left[b_3\cos\left(\alpha_1-\theta_{12}\right)\sin\left(\beta_3-\theta_{13}+\phi_H\right)+a_3\cos\left(\alpha_1-\theta_{13}\right)\sin\left(\theta_{12}-\phi_H\right)\right]} \quad (2.21)$$

$$F_H=\frac{\left\{\begin{array}{c} a_2G_3l_3\cos\left(\alpha_1-\theta_{12}\right)\cos\left(\alpha_3+\theta_{13}\right) \\ +a_3\cos\left(\alpha_1-\theta_{13}\right)\left[b_2F_S\sin\left(\alpha_2-\theta_{12}+\phi_s\right)-\left(a_2G_3+G_2l_2\right)\cos\left(\theta_{12}\right)\right] \end{array}\right\}}{a_2\left[b_3\cos\left(\alpha_1-\theta_{12}\right)\sin\left(\beta_3-\theta_{13}+\phi_H\right)+a_3\cos\left(\alpha_1-\theta_{13}\right)\sin\left(\theta_{12}-\phi_H\right)\right]} \quad (2.22)$$

2.2.2 Static Force Analysis with Virtual Work Method

2.2.2.1 Velocity Influence Coefficients

The velocity influence coefficients (VIC) of the joint variables are required when applying the VWM. VIC of the passive joint variables, s_{13} and θ_{13} are obtained by taking derivatives of Equations (2.3) and (2.4) with respect to input angle, θ_{12}:

$$\frac{ds_{13}}{d\theta_{12}}=g_{S_{13}}=\frac{a_2\cos\left(\theta_{12}-\theta_{13}\right)}{a_3\cos\left(\alpha_{12}-\theta_{13}\right)} \quad (2.23)$$

$$\frac{d\theta_{13}}{d\theta_{12}}=g_{\theta_{13}}=\frac{a_2\cos\left(\alpha_{12}-\theta_{12}\right)}{a_3\cos\left(\alpha_{12}-\theta_{13}\right)} \quad (2.24)$$

The position, and VIC of the center of mass of the crank can be calculated as:

$$\overrightarrow{A_0M_2}=\vec{r}_{M_2}=l_2e^{i\theta_{12}}\Rightarrow\begin{array}{l}\vec{r}_{M_{2x}}=l_2\cos\theta_{12}\\ \vec{r}_{M_{2y}}=l_2\sin\theta_{12}\end{array} \quad (2.25)$$

$$u_{M_2}=\frac{dr_{M_{2x}}}{d\theta_{12}}=-l_2\sin\theta_{12} \qquad v_{M_2}=\frac{dr_{M_{2y}}}{d\theta_{12}}=l_2\cos\theta_{12} \quad (2.26)$$

The position, and VIC of the center of mass of the coupler can be calculated as:

$$\begin{array}{c}\overrightarrow{A_0M_3}=\vec{r}_{M_3}=a_2e^{i\theta_{12}}+l_3e^{i\left(\theta_{13}+\alpha_3\right)}\Rightarrow\\ r_{M_{3x}}=a_2\cos\theta_{12}+l_3\cos\left(\theta_{13}+\alpha_3\right)\\ r_{M_{3y}}=a_2\sin\theta_{12}+l_3\sin\left(\theta_{13}+\alpha_3\right)\end{array} \quad (2.27)$$

$$\begin{array}{l}u_{M_3}=\dfrac{dr_{M_{3x}}}{d\theta_{12}}=-a_2\sin\theta_{12}-l_3\sin\left(\theta_{13}+\alpha_3\right)g_{\theta_{13}}\\ v_{M_3}=\dfrac{dr_{M_{3y}}}{d\theta_{12}}=a_2\cos\theta_{12}+l_3\cos\left(\theta_{13}+\alpha_3\right)g_{\theta_{13}}\end{array} \quad (2.28)$$

The position, and VIC of point *D*, which is the point of application of spring force $\vec{F}_S$, can be calculated as:

$$\vec{r}_D = b_2 e^{i(\theta_{12}-\alpha_2)} \rightarrow \begin{matrix} r_{D_x} = b_2\cos(\theta_{12}-\alpha_2) \\ r_{D_y} = b_2\sin(\theta_{12}-\alpha_2) \end{matrix} \tag{2.29}$$

$$u_D = \frac{dr_{D_x}}{d\theta_{12}} = -b_2\sin(\theta_{12}-\alpha_2) \qquad v_D = \frac{dr_{D_y}}{d\theta_{12}} = b_2\cos(\theta_{12}-\alpha_2) \tag{2.30}$$

The position, and VIC of point *E*, which is the point of application of handling force $\vec{F}_H$, can be calculated as:

$$\vec{r}_E = a_2 e^{i\theta_{12}} + b_3 e^{i(\theta_{13}+\pi-\beta_3)} \rightarrow \begin{matrix} r_{E_x} = a_2\cos\theta_{12} - b_3\cos(\theta_{13}-\beta_3) \\ r_{E_y} = a_2\sin\theta_{12} - b_3\sin(\theta_{13}-\beta_3) \end{matrix} \tag{2.31}$$

$$\begin{aligned} u_E &= \frac{dr_{E_x}}{d\theta_{12}} = -a_2\sin\theta_{12} + b_3\sin(\theta_{13}-\beta_3)g_{13} \\ v_E &= \frac{dr_{E_y}}{d\theta_{12}} = a_2\cos\theta_{12} - b_3\cos(\theta_{13}-\beta_3)g_{13} \end{aligned} \tag{2.32}$$

2.2.2.2 Virtual Work Method

To obtain the handling force, F_H, the virtual work done by the forces applied on the system are formulated as:

$$\left\{ \begin{matrix} -m_2 g v_{G_2} - m_3 g v_{G_3} + F_S\cos(\phi_S)u_D + \\ F_S\sin(\phi_S)v_D + F_H\cos(\phi_H)u_E + F_H\sin(\phi_H)v_E \end{matrix} \right\} = 0 \tag{2.33}$$

Using Equation (2.33), the handling force can be obtained as:

$$F_H = \frac{m_2 g v_{G2} + m_3 g v_{G3} - F_S\cos(\phi_S)u_D - F_S\sin(\phi_S)v_D}{\cos(\phi_H)u_E + \sin(\phi_H)v_E} \tag{2.34}$$

2.2.3 Graphical Approach for Static Force Analysis

The graphical approach requires usage of vector algebra. To obtain the unknown forces, $\vec{G}_{12}$, $\vec{F}_{32} = -\vec{F}_{23}$, $\vec{F}_{43}$ and $\vec{F}_H$, vector polygons are used. The analysis is performed for θ_{12} = 236.63° (45° from the beginning of the motion), without the lower window. In this configuration, θ_{13} = 146.01°, ϕ_S = 111.25° and ϕ_H = 158.63°. The external forces applied on the mechanism are given in Figure 2.6.

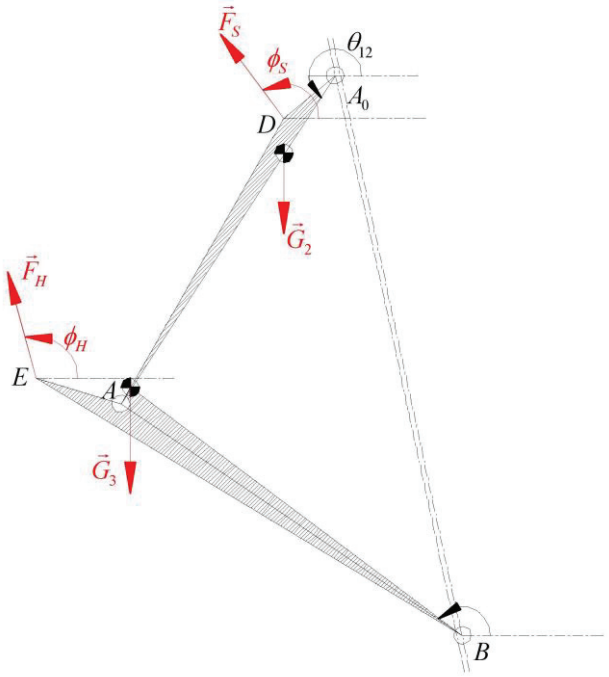

Figure 2.6. Kinematic Diagram of the Mechanism with External Forces

The first step of the analysis is to draw the free-body diagrams of the links. The free-body diagram of link 2 and 3 are provided in Figure 2.7 and Figure 2.8 respectively.

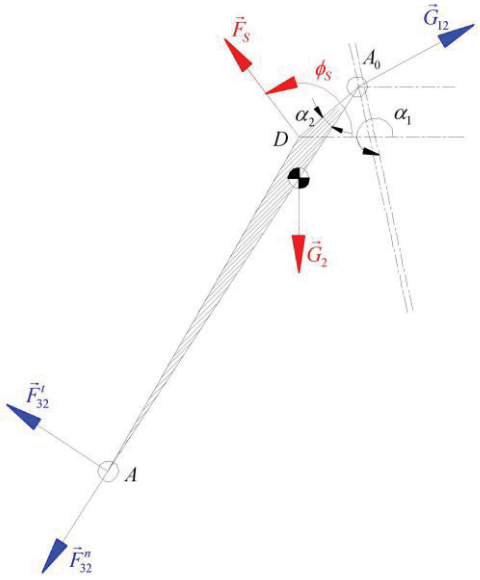

Figure 2.7. Free-body Diagram of Link 2

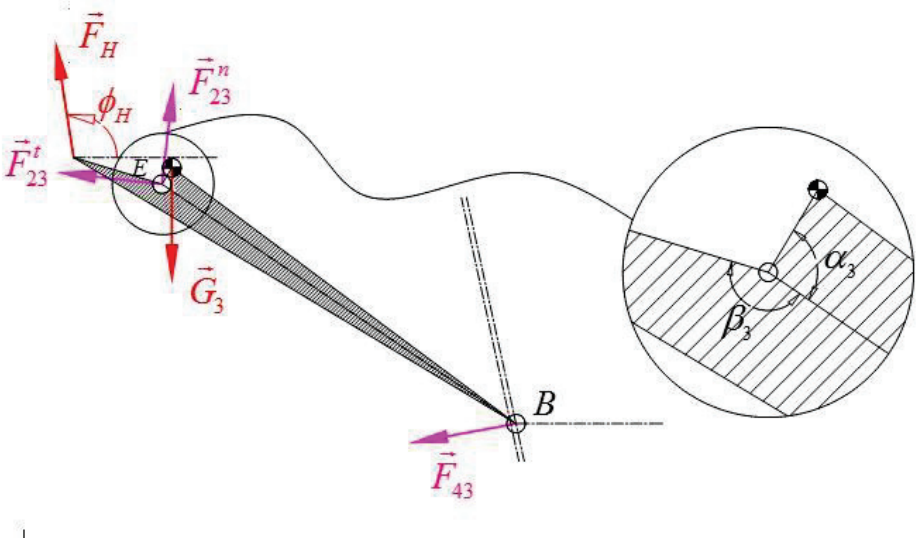

Figure 2.8. Free-body Diagram of Link 3

After obtaining the free-body diagrams with the external and reaction forces, $\vec{F}_{32}^{t}$ (link 2) is obtained from the moment equilibrium equation with respect to point A_0 as shown in Figure 2.9:

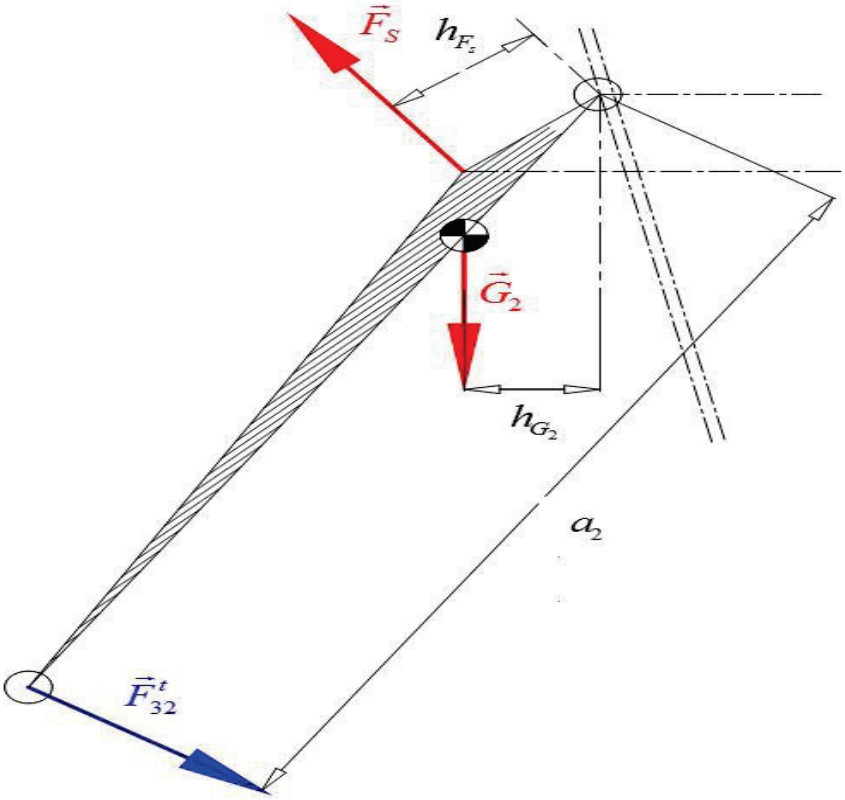

Figure 2.9. Moments About Point A_0

After the values are obtained from graphical method they are inputted in Equation (2.35).

$$\sum M_{A_0} = -F_{32}^t a_2 + G_2 h_{G_2} + F_S h_{F_S} = 0 \Rightarrow F_{32}^t = \frac{G_2 h_{G_2} + F_S h_{F_S}}{a_2} = 192.06\text{N} \qquad (2.35)$$

Then, $\vec{F}_H$ (link 3) is solved from the moment equilibrium equation with respect to point H shown in Figure 2.10. This point is chosen in order to eliminate the two unknown forces, $\vec{F}_{43}$ and $\vec{F}_{23}^n$, in the moment equilibrium condition.

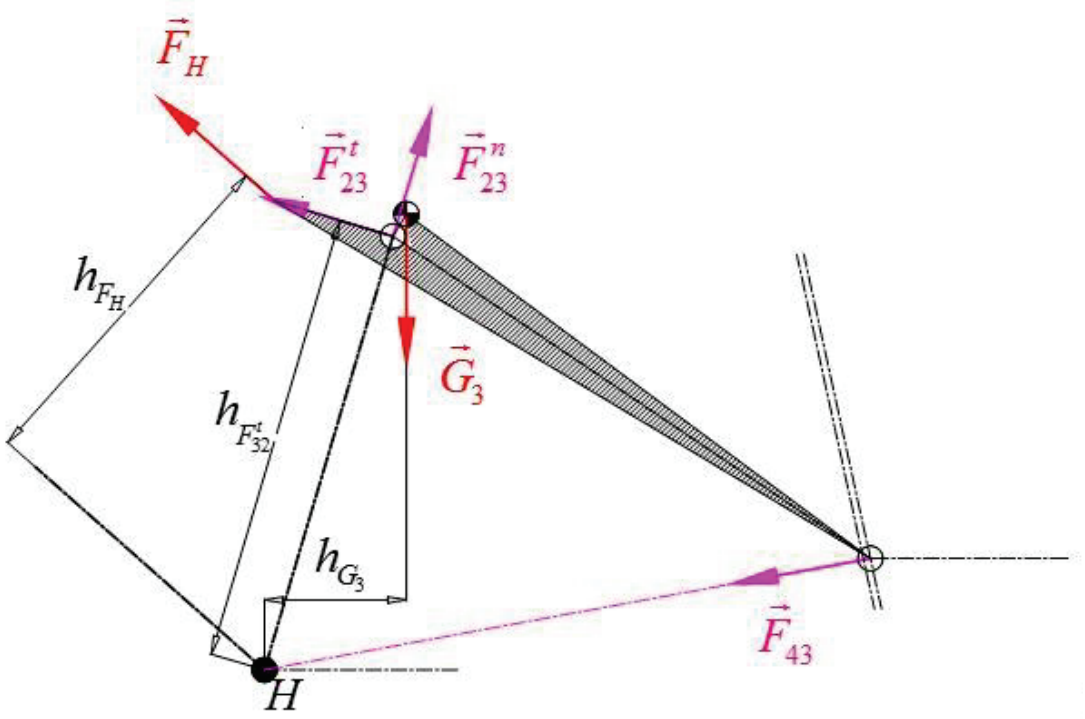

Figure 2.10. Moments About Point H

After the values are obtained from graphical method they are inputted in Equation (2.36):

$$\sum M_H = -F_{23}^t h_{F_{23}^t} + G_3 h_{G_3} + F_H h_{F_H} = 0$$
$$\Rightarrow F_H = \frac{F_{23}^t h_{F_{23}^t} - G_3 h_{G_3}}{h_{F_H}} = 105.35\text{N} \qquad (2.36)$$

The result for $\vec{F}_H$ matches with the results of the other two methods for $\theta_{12} = 236.63°$.

2.3 Numerical Results of the Static Force Analysis

The formulation developed and presented in the previous sections are used to perform the static force analysis for any position of the mechanism. The formulations are implemented to MS Excel® and required actuation forces are obtained as presented in Figure 2.10 and Figure 2.11.

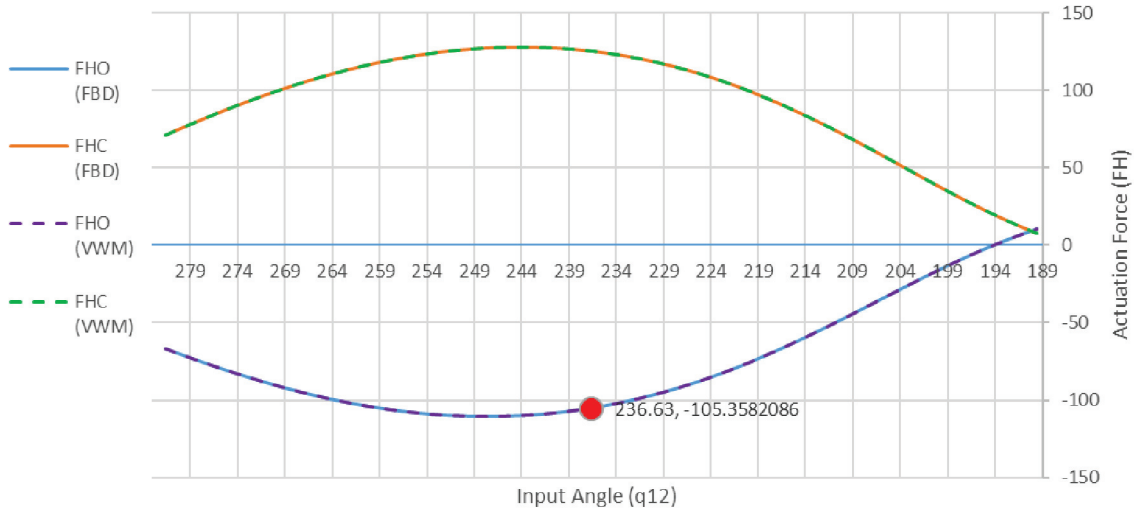

Figure 2.11. Actuation Force vs. Input Angle Without Lower Window Attached

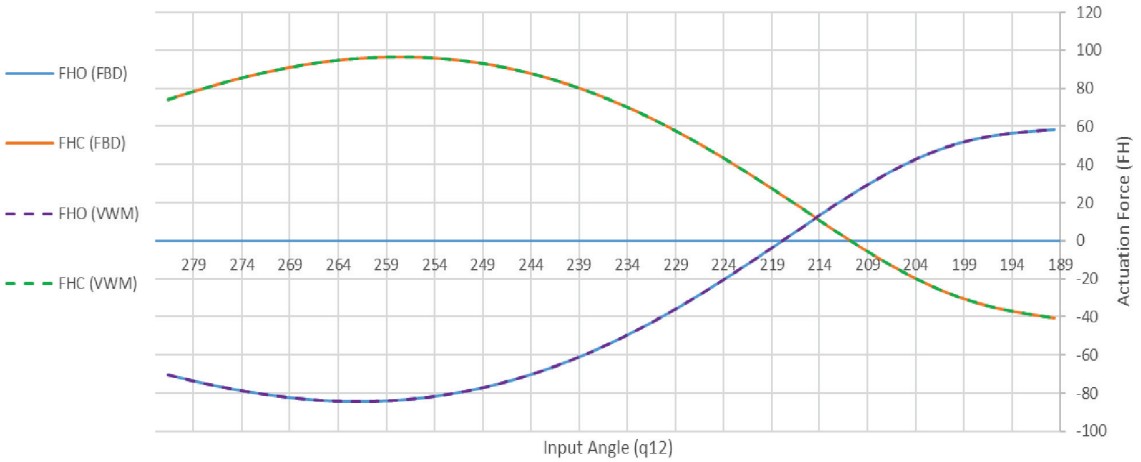

Figure 2.12. Actuation Force vs. Input Angle with Lower Window Attached

The results obtained from Newton-Euler and VWM are given in the plot for the range of 284.63°≥ θ_{12} ≥189.63° with 1° increments. The range of the input angle θ_{12} defines the mechanical limits of the mechanism with respect to the horizontal x-axis. The actuation force is obtained by using Graphical Approach for θ_{12} = 236.63° (45° from the beginning of the motion) and as it can be seen from the plot given in Figure 2.11, all the results match for each approach. The maximum closing force is found to be 128.1 N for the case without the lower window. The closing force is applied by the operator against the spring force, while the opening is basically performed by the spring force. For the case with the lower window, the maximum closing and opening forces are 96.7 N and 58.3 N, respectively.

2.4 SimMechanics Model for Force Analysis

In order to confirm the force analysis formulations and results obtained using MS Excel®, MATLAB/SimMechanics® is used. Even though SimMechanics seems not feasible for performing static force analysis, with some modifications, the results for the static force analysis of the slider crank mechanism are confirmed.

In order to create the simulation for the slider crank mechanism, firstly the structural parameters and joint displacement values for the initial position of the mechanism are defined as initial function as given in Figure 2.13.

Model initialization function:

```
tmax=3;
a2=440;
a3=463.59114323;
c0=5.58197713;
alpha1=282.2974728*pi/180;
beta2=0.55976106*pi/180;
l2=104.6;
b2=75;
alpha2=17.06*pi/180;
l3=20.9;
b3=100;
alpha3=93.09*pi/180;
beta3=162.74918717*pi/180;
m2=3.82995;
m3=16.18001;
Cx=23.6;
Cy=-257.1;
Fs2=500;
Fs1=Fs2*1.35;
Fs3=60;
Ssmin=185;
G2=m2*9.81;
G3=m3*9.81;
theta12_ini=0;
q12_ini=alpha1-beta2-theta12_ini;
s13_ini= (1/2)*(2*a2*cos(alpha1-q12_ini)+sqrt(2)*sqrt((-a2^2+2*a3^2-2*c0^2+a2^2*cos(2*alpha1-2*q12_ini)-4*a2*c0*sin(alpha1-q12_ini))));
q13_ini= atan2((a2*sin(q12_ini)-s13_ini*sin(alpha1)-c0*cos(alpha1))/a3,(a2*cos(q12_ini)-s13_ini*cos(alpha1)+c0*sin(alpha1))/a3);

Ex_ini=a2*cos(q12_ini)+b3*cos(q13_ini+pi-beta3)
Ey_ini=a2*sin(q12_ini)+b3*sin(q13_ini+pi-beta3)
Rx=-500
Ry=-500

dq13_ini = (a2*cos(alpha1-q12_ini))/(a3*cos(alpha1-q13_ini));
U_E_ini=-a2*sin(q12_ini)-b3*dq13_ini*sin(q13_ini-beta3)
V_E_ini=a2*cos(q12_ini)+b3*dq13_ini*cos(q13_ini-beta3)
psi12_ini=atan2(V_E_ini,U_E_ini)+pi
p2_ini=(Ex_ini-Rx)/cos(psi12_ini)
p1_ini=Ey_ini-Ry-p2_ini*sin(psi12_ini)
```

Figure 2.13. Initial Function Block in SimMechanics®

Following that, using the body and joint blocks available in SimMechanics® library, the mechanism is created. The block representation and the visualization of the slider crank mechanism is given in Figure 2.14.

The simulation run with 0.05 second step size and ode4 (Runge-Kutta) solver. In order to perform a static force analysis, all the links are defined as massless and their inertia tensors are assigned as zero matrices so that the effect of the inertia is cancelled. The masses are assigned as external forces acting on the center of the mass of each link by using “Body Actuator” blocks. Furthermore, the spring force is calculated by implementing the formulation given early in this chapter and applied to the system by using another “Body Actuator” block.

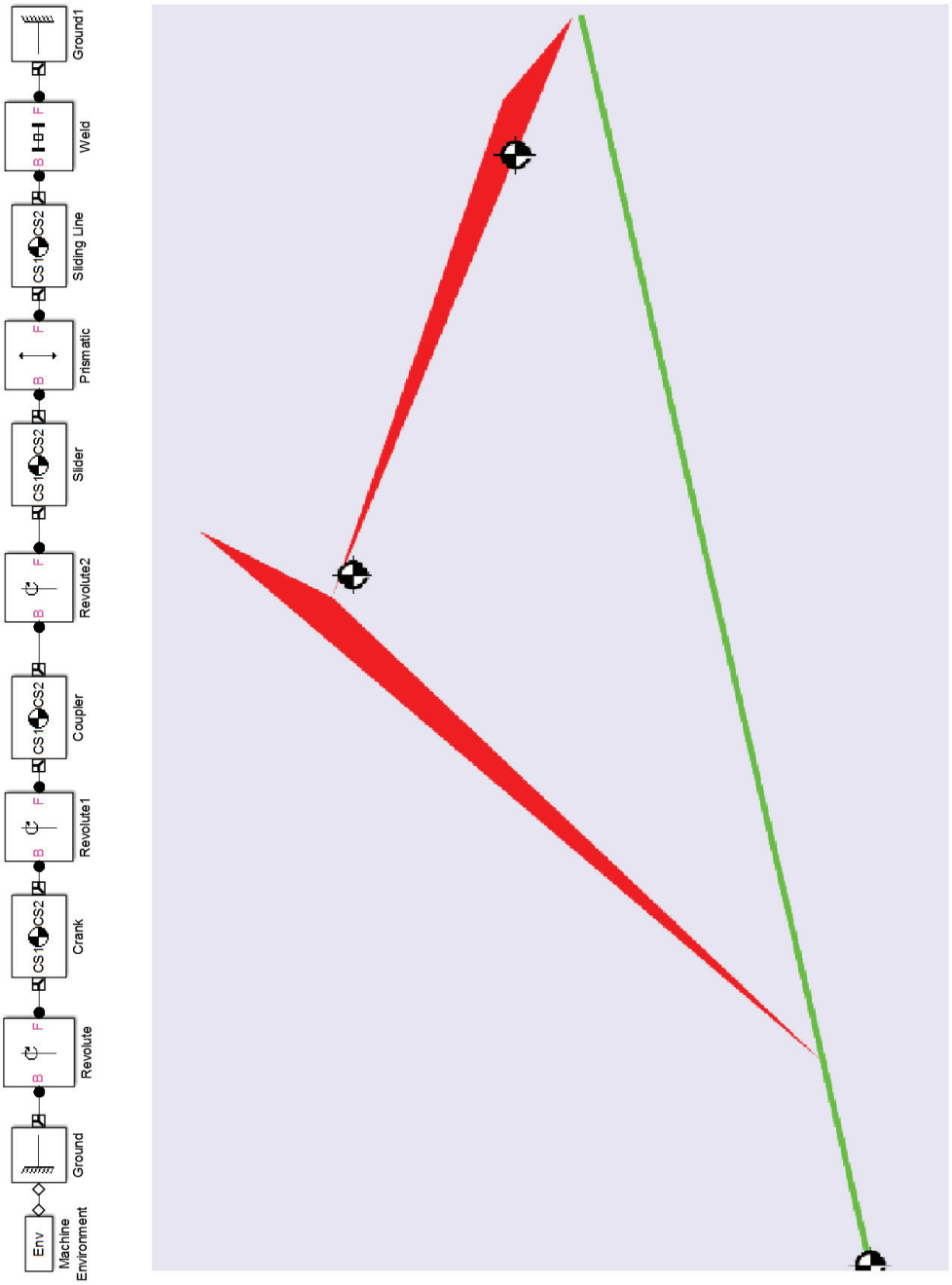

Figure 2.14. SimMechanics Model of the Existing Mechanism

Since the actuation of the real mechanism is from a body (point *E*), it is impossible to use a sensor block which calculates for the required actuation force acting on a body. In order to be able to sense the required actuation force on point *E*, another dummy mechanism is needed to be added to the original mechanism. This new mechanism attached on point *E* and the orientation of the link of the dummy mechanism

attached to the slider crank must be the same with ϕ_H. Considering these criteria, it is decided to have an PRPR as a dummy mechanism.

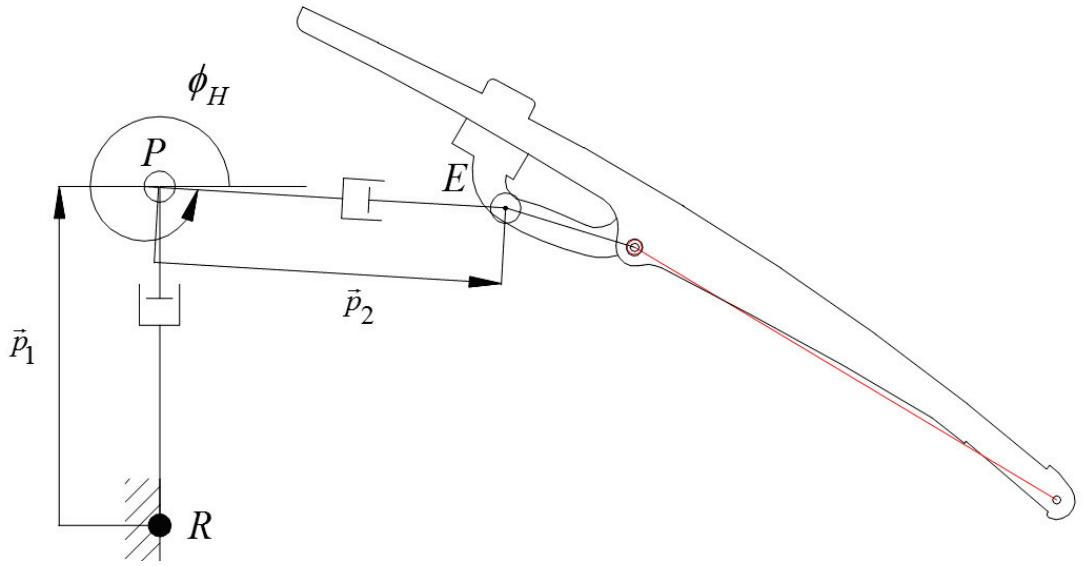

Figure 2.15. Dummy PRPR Mechanism

The position of point $R = [R_x, R_y]$ is arbitrarily assigned as R_x = -500 mm and R_y = -500 mm. Then for given positions of points E and R, and orientation of ϕ_H, the inverse kinematic analysis is done to obtain the joint variables $\vec{p}_1$ and $\vec{p}_2$. The loop equation for the PRPR mechanism is written as:

$$\begin{gathered}\overrightarrow{A_0A}+\overrightarrow{AE}=\overrightarrow{A_0R}+\overrightarrow{RP}+\overrightarrow{PE}\\ a_2e^{i\theta_{12}}+b_2e^{i(\theta_{12}+\pi-\beta_3)}=\left[R_x,\mathrm{i}R_y\right]+p_1+p_2e^{i\phi_H}\end{gathered} \tag{2.37}$$

The joint variables, $\vec{p}_1$ and $\vec{p}_2$, can be solved from Equation (2.37) as:

$$p_2=\frac{a_2\sin\theta_{12}+b_2\sin\left(\theta_{12}+\pi-\beta_3\right)-R_y}{\sin\phi_H} \tag{2.38}$$

$$p_1=a_2\cos\theta_{12}+b_2\cos\left(\theta_{12}+\pi-\beta_3\right)-R_x-p_2\cos\phi_H \tag{2.39}$$

This dummy mechanism is added to the original one in the SimMechanics® environment and it is presented in Figure 2.16. In order to sense the required force input at point E, the actuation is given as motion input from the prismatic joints of the PRPR mechanism. Then, a body sensor which measures the reaction force occurring at point E, (at the contact between the slider crank and PRPR mechanism). This sensed reaction force

also represents the required actuation force by the mechanism. The data obtained from the body sensor and calculated actuation force to open the mechanism are subtracted from each other and the error is calculated to be in the order of 10^{-7} N, which is negligible.

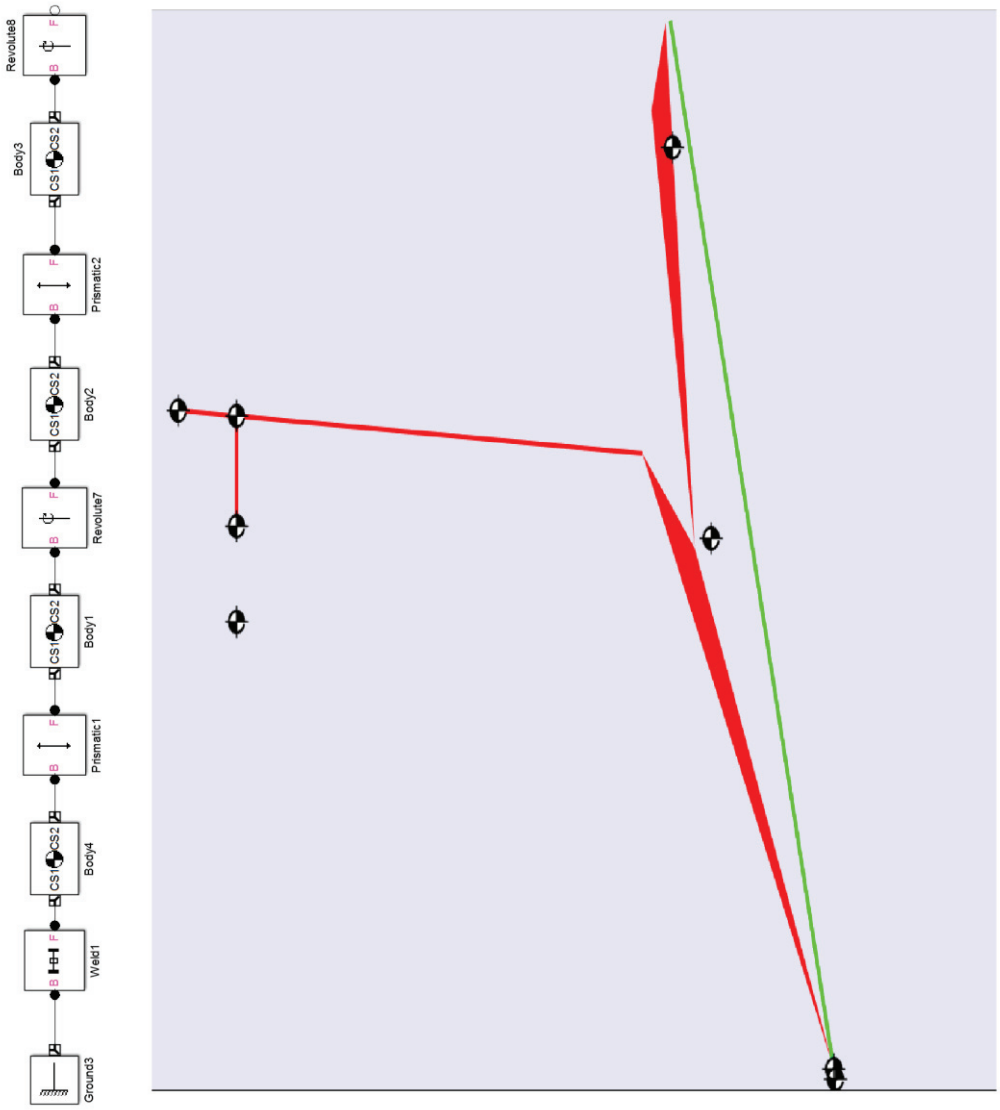

Figure 2.16. SimMechanics Model of the Dummy Mechanism

In order to validate the assumption that the inertial effects are negligible also dynamic SimMechanics model comprising all inertia properties of the links is built. The opening force for the case without the lower window for kinematic and dynamic simulation are presented in Figure 2.17. As it can be seen from the figure, the difference is negligible.

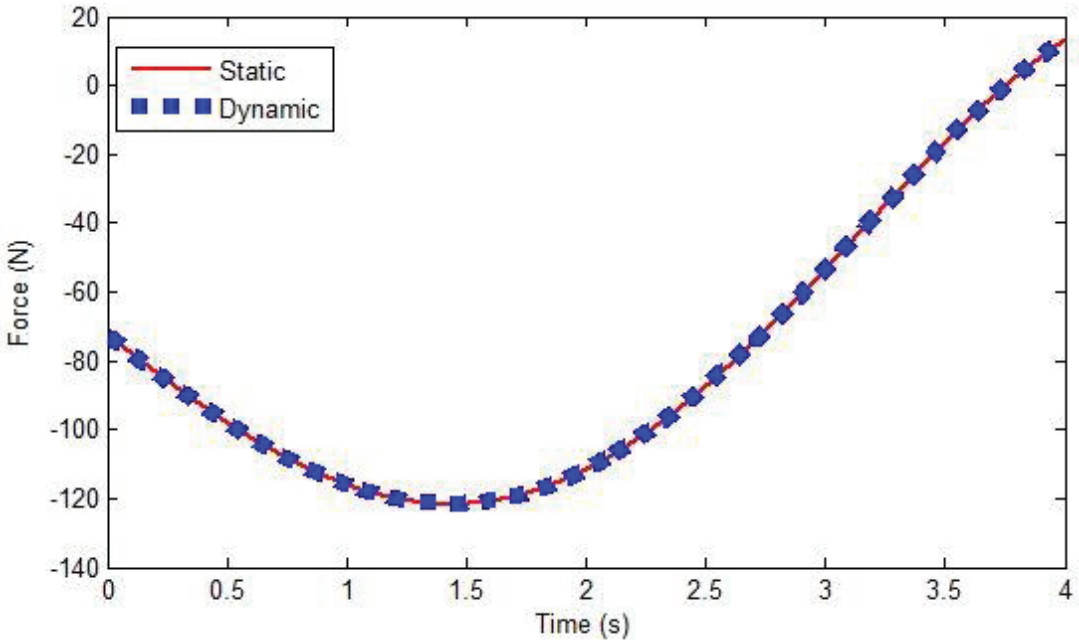

Figure 2.17. Dynamic and Static Simulation Results for the Opening Force Without the Lower Window

The difference between the handling forces for the dynamic and static simulations is given in Figure 2.18. The difference represents the contribution of the inertial forces to the handle force and the difference is less than 0.4 N.

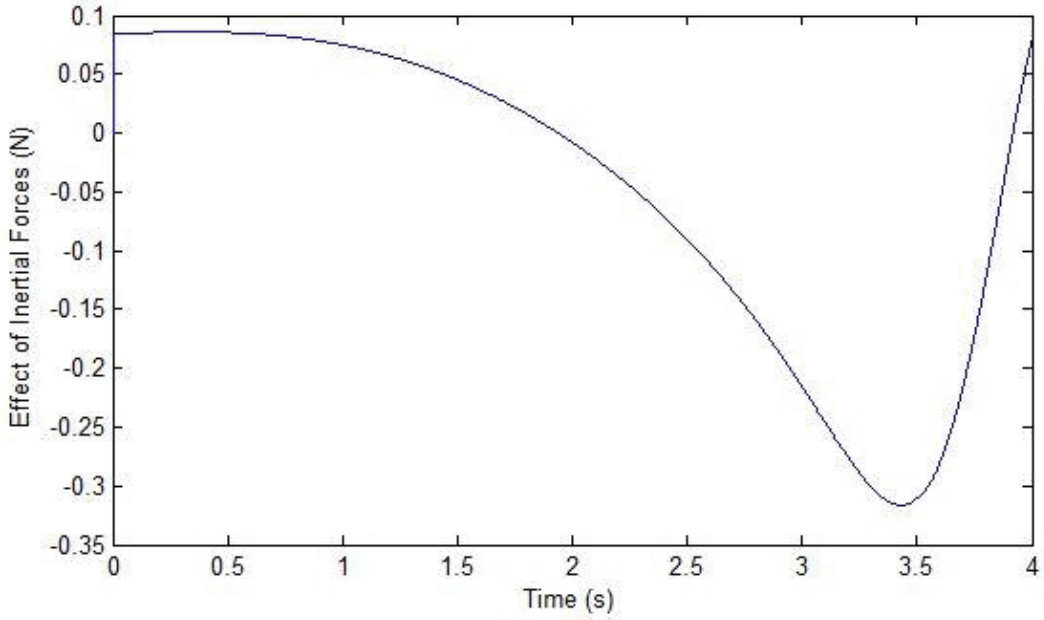

Figure 2.18. Difference Between Handling Forces for the Dynamic and Static Simulations

CHAPTER 3

SOLUTION ALTERNATIVES

In CHAPTER 2, the static force analysis is presented. At the end of this analysis, the values of required handling force, F_H, for actuating the mechanism is presented in Figure 2.11. This analysis is performed for the existing configuration of the mechanism used in the cabin of an earth moving machinery. In this chapter, the aim is to obtain a smaller actuation force by changing the configurations of the mechanism. These configurations are the position of the spring, type of the spring, length of the links and handle position.

3.1 Spring Position Variation

In this section, a smaller actuation force is sought by changing the assembly points of the spring (points C and D in Figure 2.1). To calculate the handling force for varying attachment points of the current spring on the mechanism, an algorithm is implemented in MS Excel® environment. The algorithm takes the length constraints of the spring as input. For the existing spring attached on the actual mechanism, the maximum length is $S_{S_{\max}} = 285$ mm, the minimum length is $S_{S_{\min}} = 185$ mm as previously given in Section 2.2.

To parametrize the positions of points C and D, which are the assembly points of the spring, d_1, k_1, d_2 and k_2 dimensions are used as presented in Figure 3.1. The handling force is calculated for varying d_i and k_i values for $i = 1, 2$.

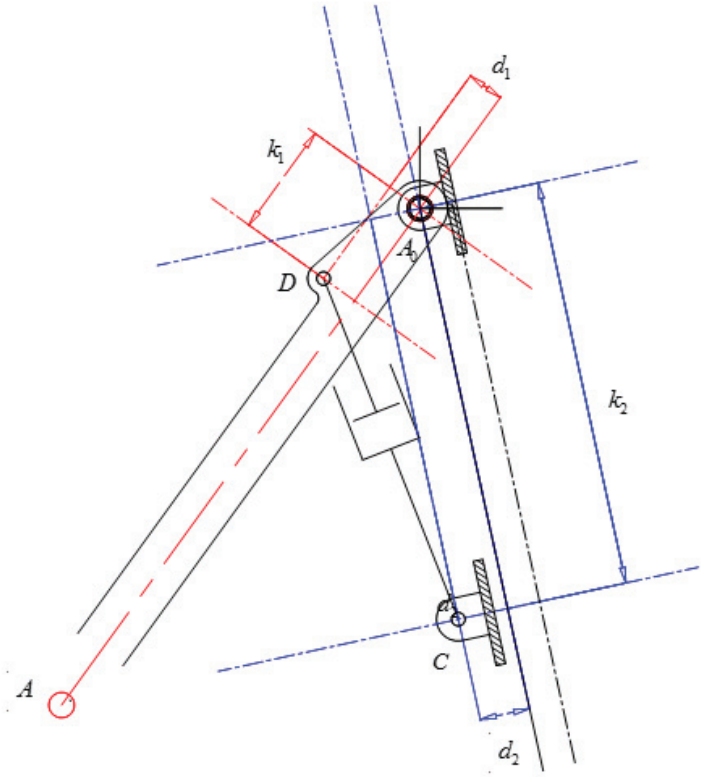

Figure 3.1. Spring Position Parameters

For any k_1 and k_2 values, the positions of points C and D are calculated for any position of the mechanism. Using those positions, the length (S_S) and orientation (ϕ_S) of the spring are obtained. Then, a check is performed to see if the length of the spring exceeds $S_{S_{\max}}$ and $S_{S_{\min}}$ at any instant. If the length constraint of the spring is satisfied, the spring force, F_S is calculated using Equations (2.7) and (2.8). Following that, all actuation force (F_H) values at any instant of the mechanism for any k_1 and k_2 values are calculated. Then, the maximum values of the actuation force for the certain values of k_1 and k_2 are extracted and stored in a table in the Excel® worksheet. Using that table, the suitable configuration for k_1 and k_2 values are chosen. After this some fine tuning is done manually to the d_i values since their limits are very low but they give significant change in the results. Figure 3.2 and Figure 3.3 present the actual actuation

force values and the minimized force values by changing k_1 and k_2. It is clearly seen from the figure that, changing the position of the spring affects the resulting actuation force.

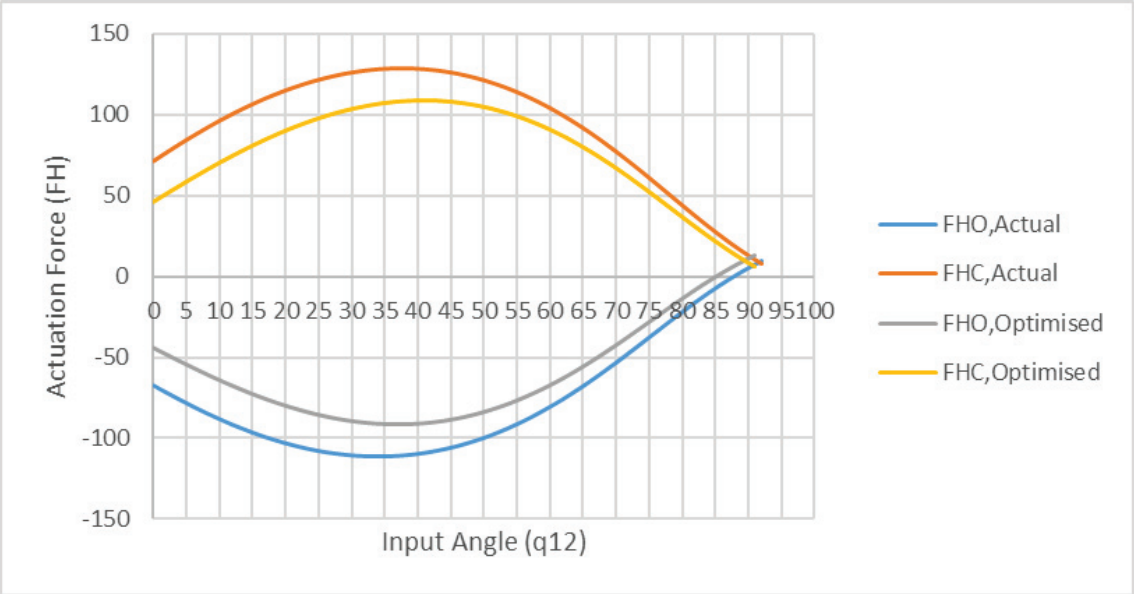

Figure 3.2. Actuation Force for Actual and Chosen k_1 and k_2 Values Without the Lower Window

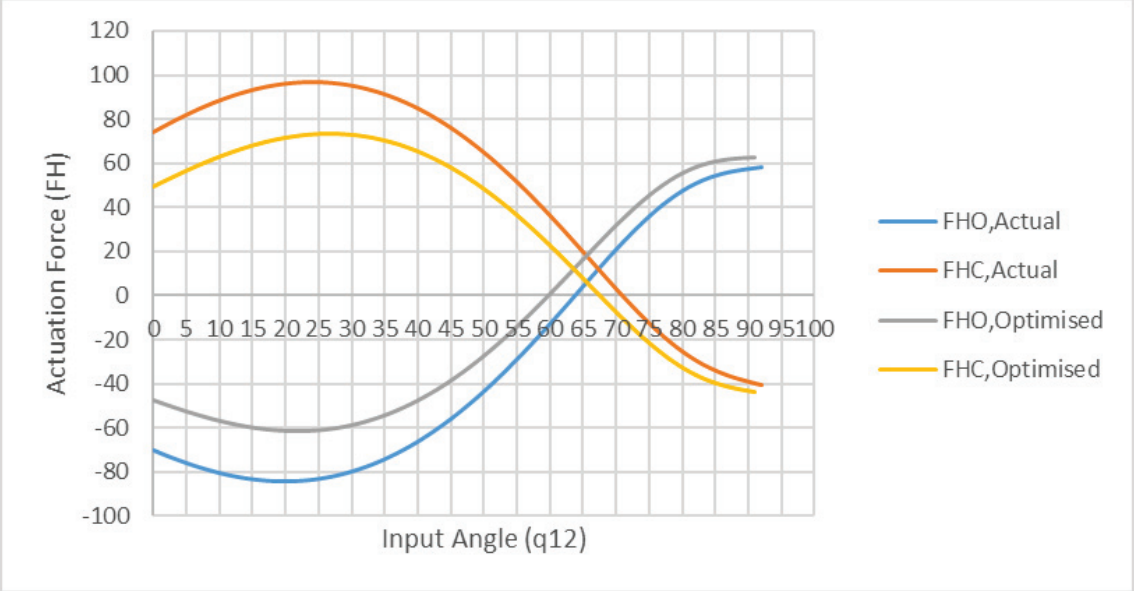

Figure 3.3. Actuation Force for Actual and Chosen k_1 and k_2 Values With the Lower Window

For the case without the lower window the maximum closing force is decreased to 109 N, whereas it was 128.1 N in the original design. For the case with the lower window, the maximum closing force is decreased from 96.7 N to 73.4 N and the opening force increased from 58.3 N to 62.9 N.

3.2 Link Length Optimization

In order to optimize the length of the links, 2-position synthesis is performed. The first constraint is retaining the first and last position of the coupler link (a_3). So, for the synthesis, these parameters along with the length of the coupler link (a_3) are taken as the inputs. The purpose of this task is to find the suitable crank length and fixed point position. At the beginning of the calculation, the position of point B_1 and B_2 of the coupler on the sliding line and the orientation (θ_{13}) are known so the positions of points A_1 and A_2 are calculated as follows:

$$\begin{aligned} A_1 &= B_1 + a_3 e^{i\theta_{13\min}} \\ A_2 &= B_2 + a_3 e^{i\theta_{13\max}} \end{aligned} \tag{2.40}$$

After that $\left|A_1 A_2\right|$ line is drawn and the middle point A_{mid} is found. At this point, a perpendicular line is drawn to $\left|A_1 A_2\right|$ line and fixed point (A_0) lies on that perpendicular line. Another input (ΔL) is introduced which defines the distance between points A_{mid} and A_0. To calculate the position of the fixed point (A_0) the following formulas are used:

$$\begin{aligned} m &= \frac{A_{1_x} - A_{2_x}}{A_{2_y} - A_{1_y}} \\ A_{0_x} &= A_{mid_x} + \Delta L \\ A_{0_y} &= A_{mid_y} + \Delta L m \end{aligned} \tag{2.41}$$

Finally, we can find the length of the crank a_2 with the following formula

$$a_2 = \sqrt{\left(A_{0_x} + A_{1_x}\right)^2 + \left(A_{0y} + A_{1_y}\right)^2} = \sqrt{\left(A_{0_x} + A_{2_x}\right)^2 + \left(A_{0y} + A_{2_y}\right)^2} \tag{2.42}$$

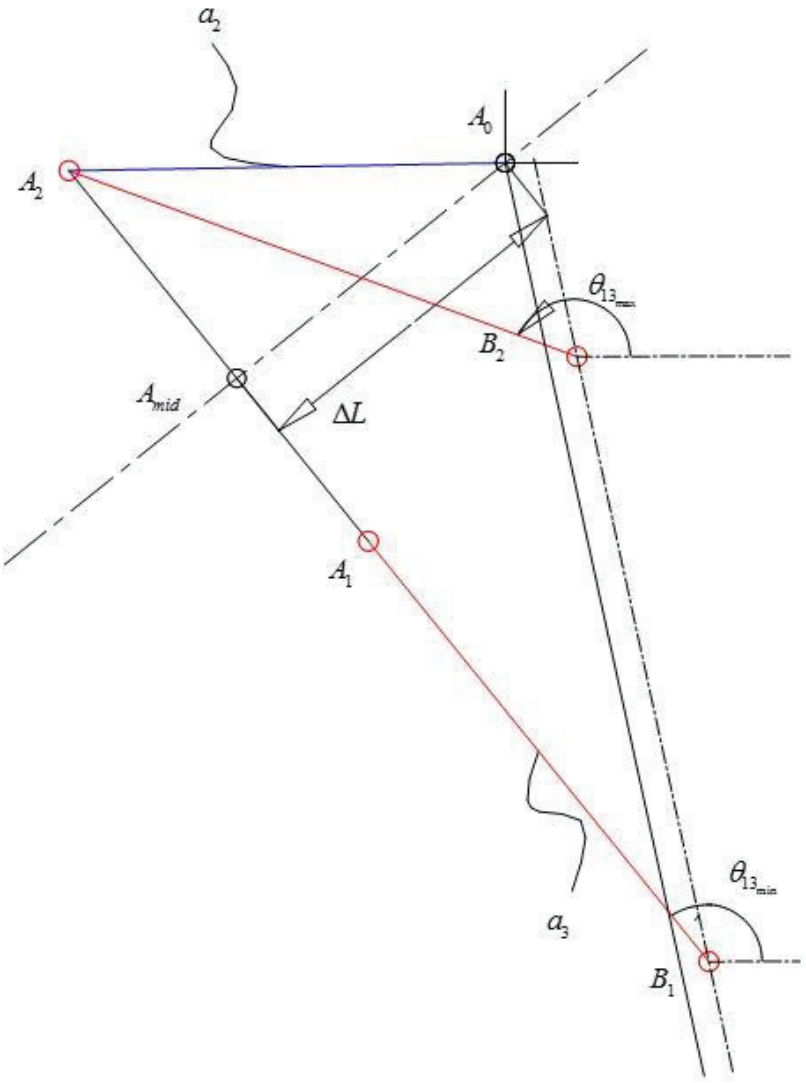

Figure 3.4. Two Point Synthesis

All the formulas given above are implemented in Excel®. With the changing input parameter a_3 it is observed that there is no overall minimization of the force curve. As given in Figure 3.5 for smaller or larger values of a3 different parts of the curve improve.

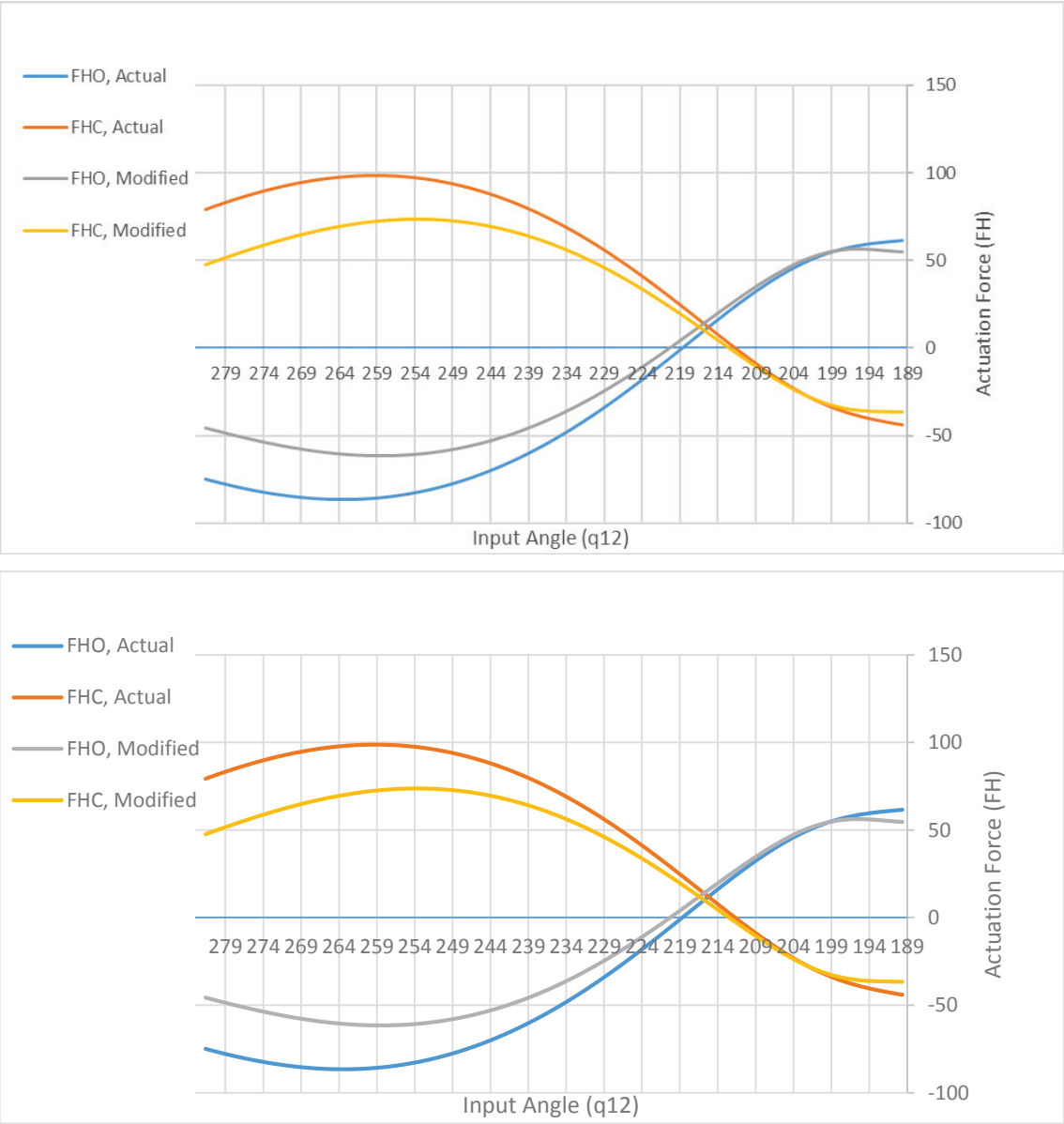

Figure 3.5. Actuation Force for Actual and Chosen a_3 Values

3.3 Handle Position Optimization

An attempt to optimize the position of the handle is performed. The location of point E, which is the point where the handle force is applied, is parametrized and a check on the required actuation force has been performed. Due to constructional constraints of the mechanism, w_1 and w_2 terms in Figure 3.6 are introduced instead of b_3 and β_3. Again due to the constructional constraints, the value of w_1 is constant and with the changing

value of w_2, the required actuation force is calculated. The results showed that there is no decrease in the required actuation force with the increasing value of w_2. The decrease in the required actuation force is observed only when w_2 decreases. However, due to constructional constraints, this minimization for the actuation force is not appropriate for the problem.

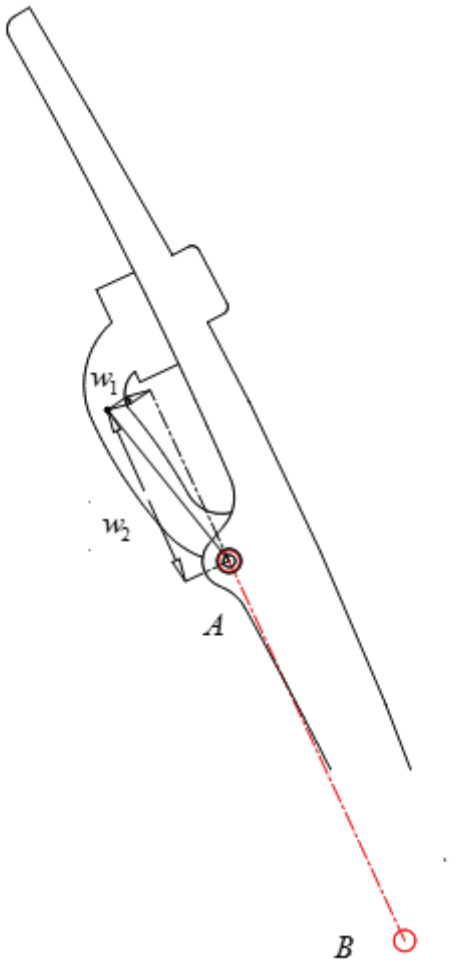

Figure 3.6. Handle Position Parameters

CHAPTER 4

TEST SETUP AND RESULTS

In this chapter, the modifications applied on the current front window mechanism, the test setup and the results obtained from the tests are presented.

4.1 Applied Modifications on the Current Mechanism

The results obtained from analysis done in the precious chapters showed that only spring position optimization is feasible for a test procedure considering the demands/resources of Mecalac Turkey. Figure 4.1 represents the current front window mechanism attached on the earth moving machinery. To minimize the required actuation force using spring position optimization, some modifications are applied on the slot shown in Figure 4.2.

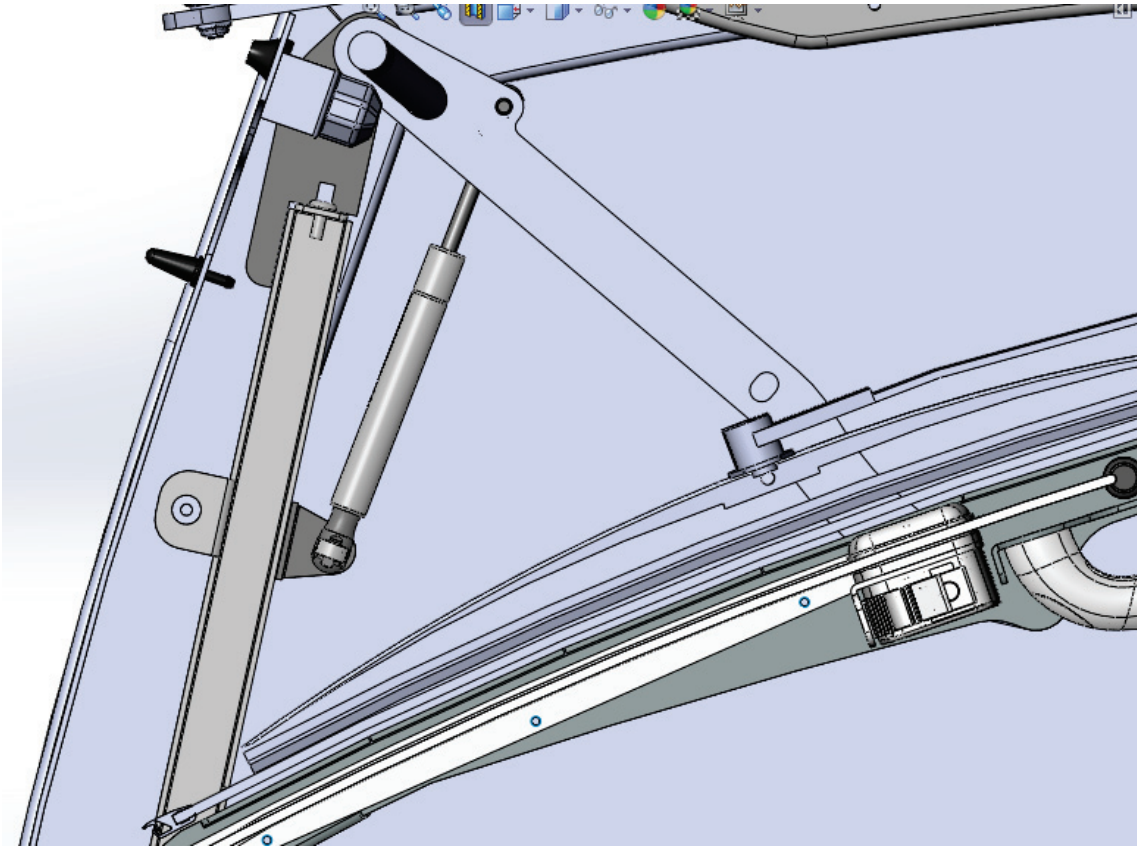

Figure 4.1. Current Front Window Mechanism

Figure 4.2 represents the original version and modified version of the slot. As it can be seen from Figure 4.2, the attachment point of the spring on the slot is modified so that the required actuation force is minimized.

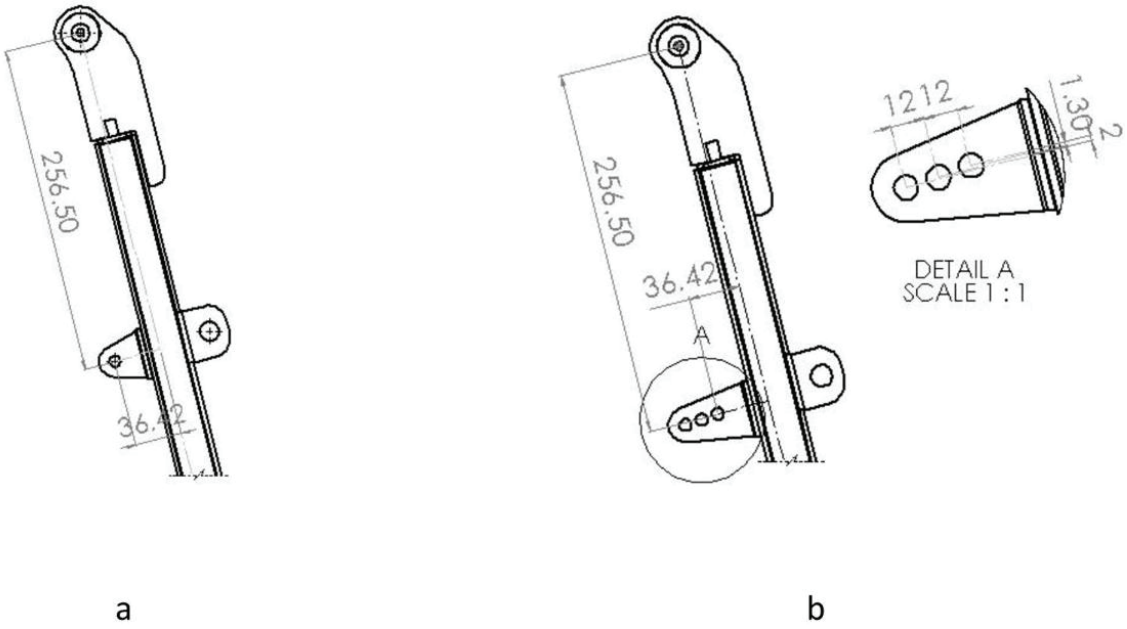

Figure 4.2. Technical Drawing of the Slot: a) Original, b) Modified version

The attachment point of the spring on the slot is a welded part on slot, so the original attachment point is cut from the slot and the modified version is welded.

4.2 Test Setup

In order to measure the manual actuation force on the mechanism a force sensor is needed. Since the position and orientation of the force exerted on the mechanism by the operator is important for reproducing the calculated forces, the force sensor should not be large in size and change the position of application of the force. At the same time, the force sensor should measure at least 150 N of force in x-, y- and z-directions. Considering these criteria, a force/torque transducer of ATI Industrial Automation with brand mini45 is selected due to its compactness and high force capabilities (Figure 4.3). The force sensor has ±580 N range in x- and y-directions and ± 1160 N in z-direction (normal to the planar face of the device). Physical specifications of the device are declared as 0.0917 kg mass, 45 mm diameter, 15.7 mm height.

Figure 4.3. Mini 45 Transducer

The force sensor is connected to a data acquisition unit, Net Box, with a transducer cable that delivers power from the Net Box, shown in Figure 4.4 and transmits the strain gage data to the Net Box. The primary function of the Net Box is to process and communicate the transducer's force readings to a computer. Communication can be done through ethernet, EtherNet/IP and CAN bus. In this specific application ethernet connection is selected. The strain gage data that is delivered to the Net Box is then processed in the device according to the calibration matrix that is already embedded in the Net Box. This calibration of mini45 transducer is according to the code US-120–160 / SI-580–20.

Figure 4.4. ATI Industrial Automation's Net Box

Net FT system is connected to the user's PC through the ethernet port via the M12 to RJ45 adapter and an ethernet cable. Once the cable connection is done, a point-to-point connection is configured between PC ethernet interface and Net FT ethernet interface. This configuration allows user to have least amount of data loss and lowest latency. IP address of the NET FT is configured using the DIP switches. DIP switch 9 sets the IP to 192.168.1.1. Once this is done, and the configuration of the TCP/IP connection is made using the data given in the datasheet, force data can be exported from the IP over a specified port by providing the calibration code and the intended metric unit as an Excel datasheet. This final step of the acquisition of the force readings is done within the NET FT's interface shown in Figure 4.5.

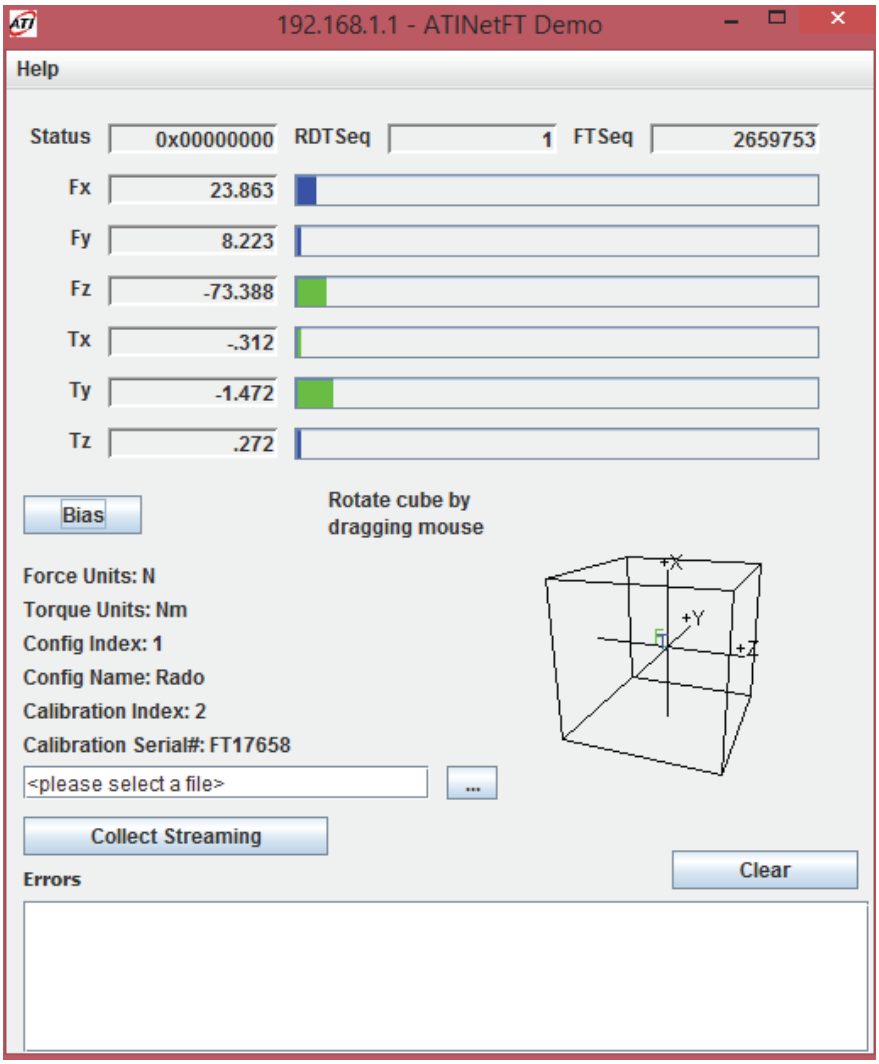

Figure 4.5. NET F/T Interface

As mentioned before in order to have accurate measurements, the sensor has to be attached to the mechanism such that it doesn't change the point of the application of force. Furthermore, the whole force used to actuate the mechanism has to flow through the sensor. The only solution found to overcome these issues is to design and produce an extra part on which the sensor is attached. This part causes a shifting of the force in perpendicular direction to the plane of the mechanism so that this shifting does not affect the force characteristics. The designed part connects the frame of the window and the sensor as shown in Figure 4.6. On the other side of the sensor, the handle where the force is applied is attached as shown in Figure 4.7.

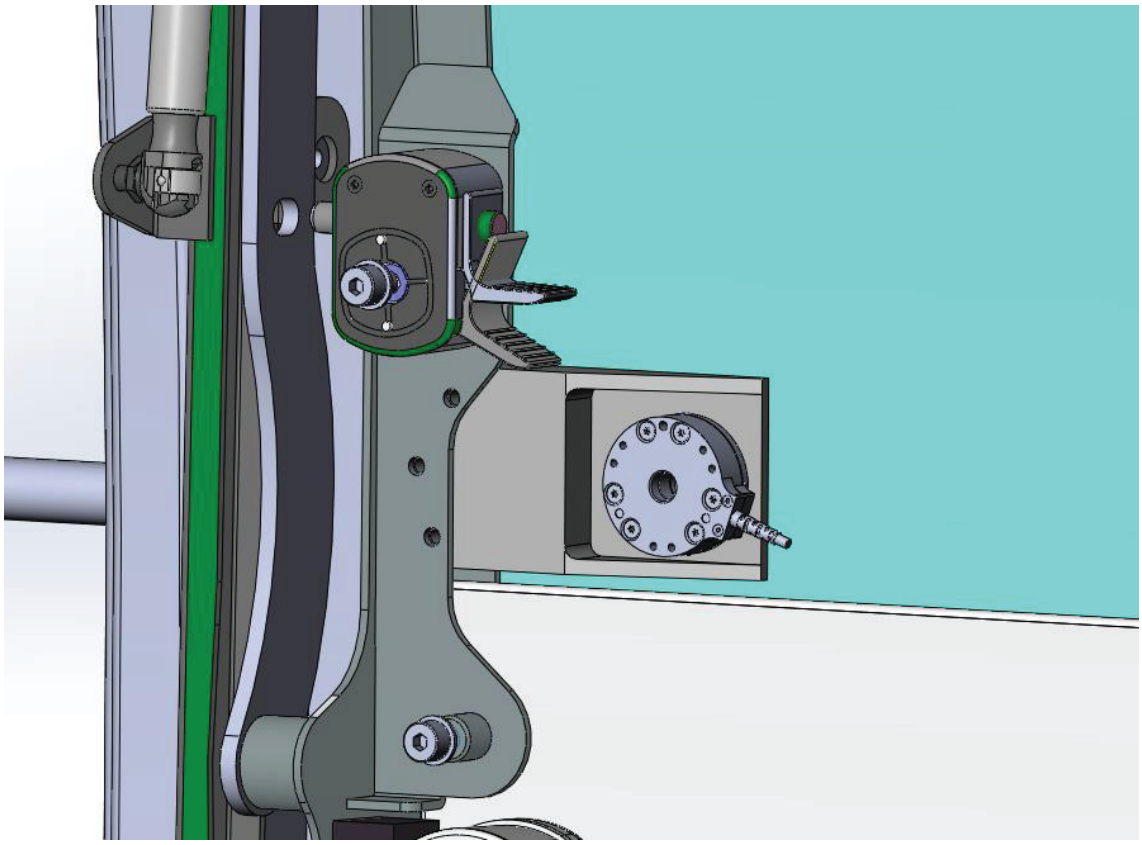

Figure 4.6. Sensor Attaching Point

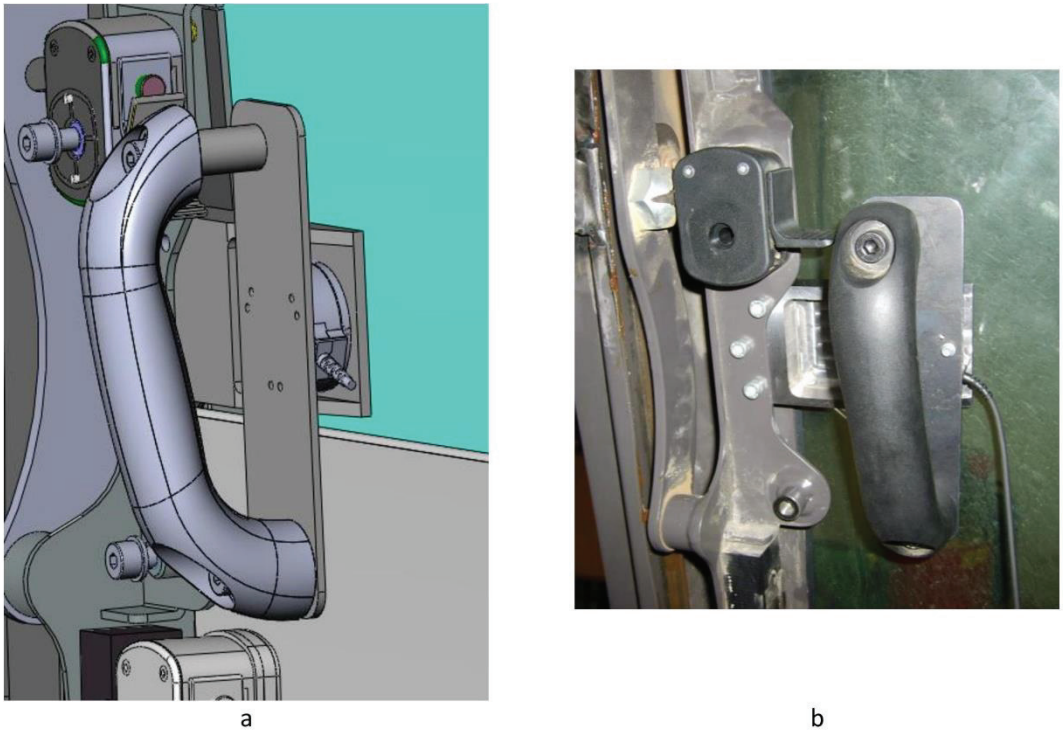

a b

Figure 4.7. Complete Sensor Assembly: a) CAD Model, b) Photo of Actual System

To measure the angular displacement of the crank during the motion an encoder is used. The encoder's brand is AMS and the model AS5045 which is a 12-bit programmable magnetic rotary position sensor presented in Figure 4.8. Measurements are done when a simple two-pole magnet rotates over the center of the chip.

Figure 4.8. AMS AS5045 Encoder and Magnet

To get the data from the sensor a data acquisition card (DAQ) whose brand is Humusoft and model is MF624 is used as shown in Figure 4.9. This DAQ card is a PCI multifunction I/O card.

Figure 4.9. Humusoft MF624 DAQ Card

The encoder is connected to the DAQ card which is connected to a PC. Matlab Simulink® is used as the user interface. The signal that is obtained from the encoder through the DAQ card is processed in this interface using the blocks available in the Simulink® library. To be able to synchronize the data obtained from the force sensor and the data obtained from the encoder computer's real time is used. The model built reads the computer time, processes the encoder data and finally stores the displacement value as well as the computer time in the workspace as shown in Figure 4.10.

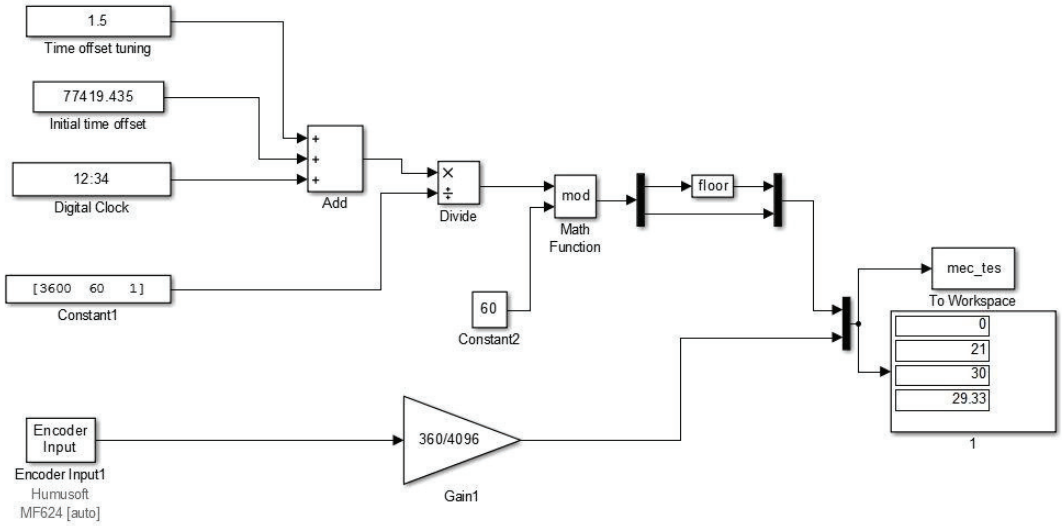

Figure 4.10. Simulink® Model for Encoder Data

To attach the encoder to the mechanism two parts are needed to be produced by a 3D printer. The first part is used to attach the magnet on the fixed link and the second one is used to attach the encoder on the crank as shown in Figure 4.11.

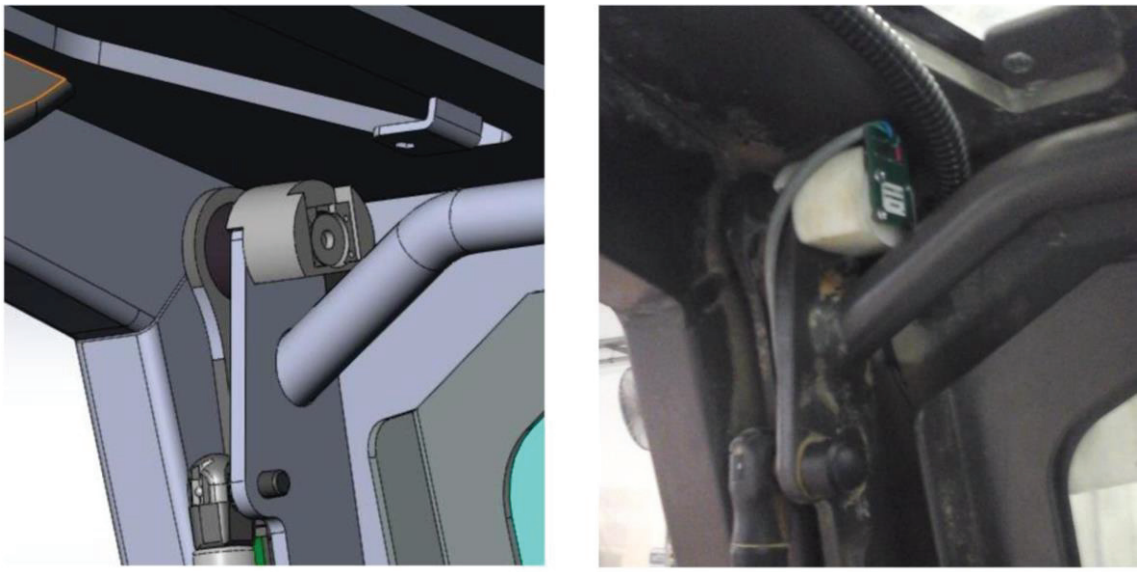

Figure 4.11. Complete Encoder Assembly: a) CAD Model, b) Photo of Actual System

4.3 Test Results

The test results given are the data taken from the force sensor and encoder. For every configuration of the mechanism (with or without the lower window) in each direction of motion (opening or closing the window) measurements are taken. Both sensor data were combined considering to the clock time and position vs. force graphs were drawn. Since the manual force exerted on the system cannot be the same for each measurement, the average of the peak force for each measurement per configuration and direction is taken as a result. Afterwards the results from the original and modified spring position are compared for each configuration and direction of motion respectively and they are given in Table 4.1. In Table 1, x-axis of the force sensor is parallel to the handle (and hence the window) and z-axis is normal to the handle. For opening, the critical part is at the end of the motion (see Figure 2.12), where the tangent to the handle point trajectory is normal to the handle. Therefore, the z-component of the measured data is considered for opening. On the other hand, for closing, the critical party is right after the half of the motion (see Figure 2.11), where the tangent to the handle point trajectory is parallel to the handle. Therefore, the x-component of the measured data is considered for closing.

Table 4.1. Average Maximum Force Comparison for All Configurations and Directions of Motion

Configuration	Without the Lower Window Attached		With the Lower Window Attached	
Direction of Motion	Opening	Closing	Opening	Closing
Calculated for original mechanism	Not critical	128.54 N	58 N	97.1 N
Calculated for modified mechanism	Not critical	110 N	61.1 N	73.8 N
Axis	z	x	z	x
Original Spring Position	125.82 N	124.69 N	238.62 N	68.4 N
New Spring Position	123.4 N	123.18 N	223.57 N	60.83 N

The measured maximum force values mostly comply with the estimated force values via calculations during closing. A big difference between the measured and calculated values appear during opening of the mechanism. The reasons for that are the dimensional differences of the CAD model and the real mechanism, and the force model of the spring. Especially, it is observed that during the opening motion the pneumatic spring does not perform according to its performance values in its datasheet, which may be due to performance decrease in time and environmental conditions such as temperature.

Furthermore, from the results obtained the work done manually in each configuration and direction of motion was calculated. For the mathematical model, the work done is calculated by multiplying the corresponding horizontal and vertical components of the calculated required manual force and the handle point displacements and summing up: $\sum_{\theta_{12}} F_H \left[\cos(\phi_H) u_E + \sin(\phi_H) v_E \right] \Delta\theta_{12}$ .For the measured data, the same formula is used for calculating the work where the force components $F_H \cos(\phi_H)$ and $F_H \sin(\phi_H)$ are evaluated by making use of coordinate transformations form the sensor coordinates to the global horizontal and vertical coordinates. The results show that the

work done in the real system is lower than the calculated one as shown in Table 4.2. Also they show that the work done in the calculations and in the real modified system is lowered with respect to the original one.

Table 4.2. Average Work Comparison for All Configurations and Directions of Motion

Configuration	Without the Lower Window Attached		With the Lower Window Attached	
Direction of Motion	Opening	Closing	Opening	Closing
Calculated for the original mechanism	-51.23 N·m	63 N·m	-22.1 N·m	34 N·m
Calculated for modified mechanism	-43.5 N·m	54.7 N·m	-14.4 N·m	25.6 N·m
Original Spring Position	9.5 N·m	64.5 N·m	19.1 N·m	-25.8 N·m
New Spring Position	11.3 N·m	57 N·m	14.9 N·m	-18 N·m

The results given in Figure 4.12 and Figure 4.13 are the measured manual actuation forces for opening the mechanism without the lower window attached. During this motion, most of the work is done by the spring. Manual force is required at the end of the motion to lock the mechanism in the open position. In the tests, larger force requirements are measured towards the end of the motion, which appear in the z-direction (normal to the handle). As it can be seen during the motion also there are force requirements which are the uncontrolled resistive force done by hand. Opening the window without the lower window is not a critical point, so in this case we don't seek any improvements and the average results show that the force is not much changed.

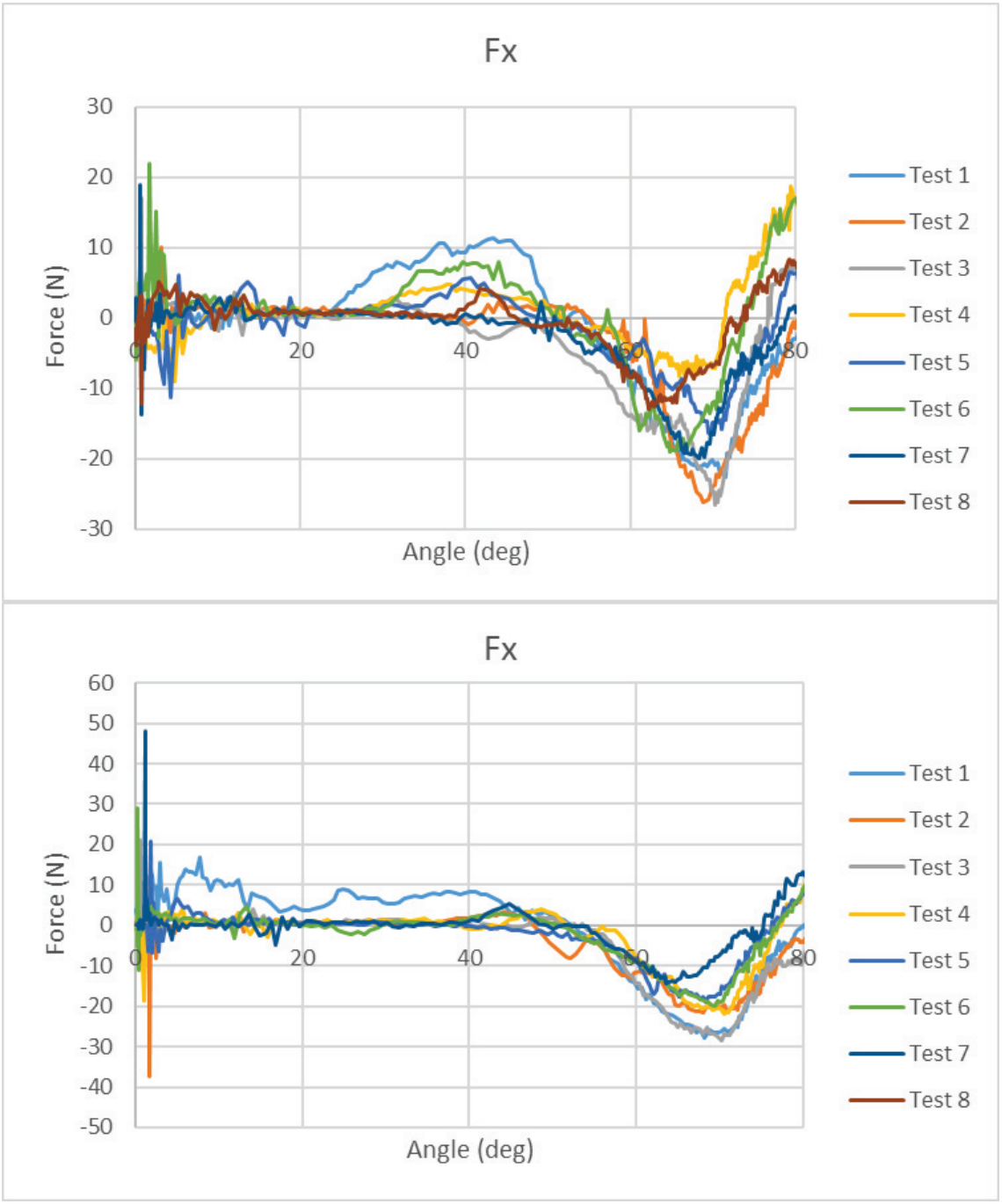

Figure 4.12. Required Actuation Force for Opening the Mechanism Without The Lower Window (Existing and Modified Spring Position)

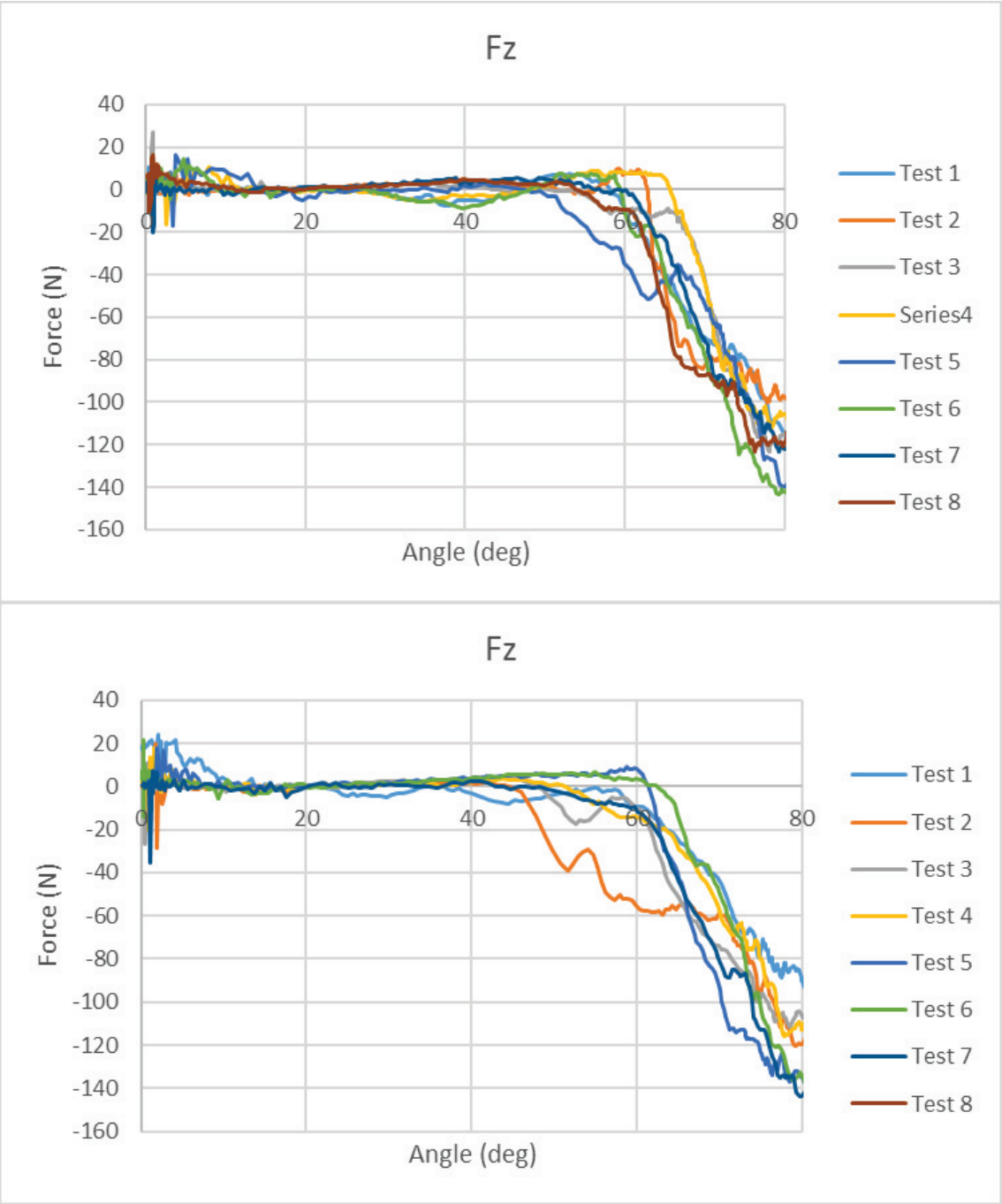

Figure 4.13. Required Actuation Force for Opening the Mechanism Without The Lower Window (Existing and Modified Spring Position)

The main problem with the case without the lower window is in the closing direction, where the operator mainly does work against the spring. As seen from the measurement data in Table 4.1, in x-axis (parallel to the window – approximately tangential to the hand trajectory) there is no improvement in terms of decreasing the

necessary force considering the original and modified spring position. The results of measurements for closing direction of motion are presented in Figure 4.14 and Figure 4.15.

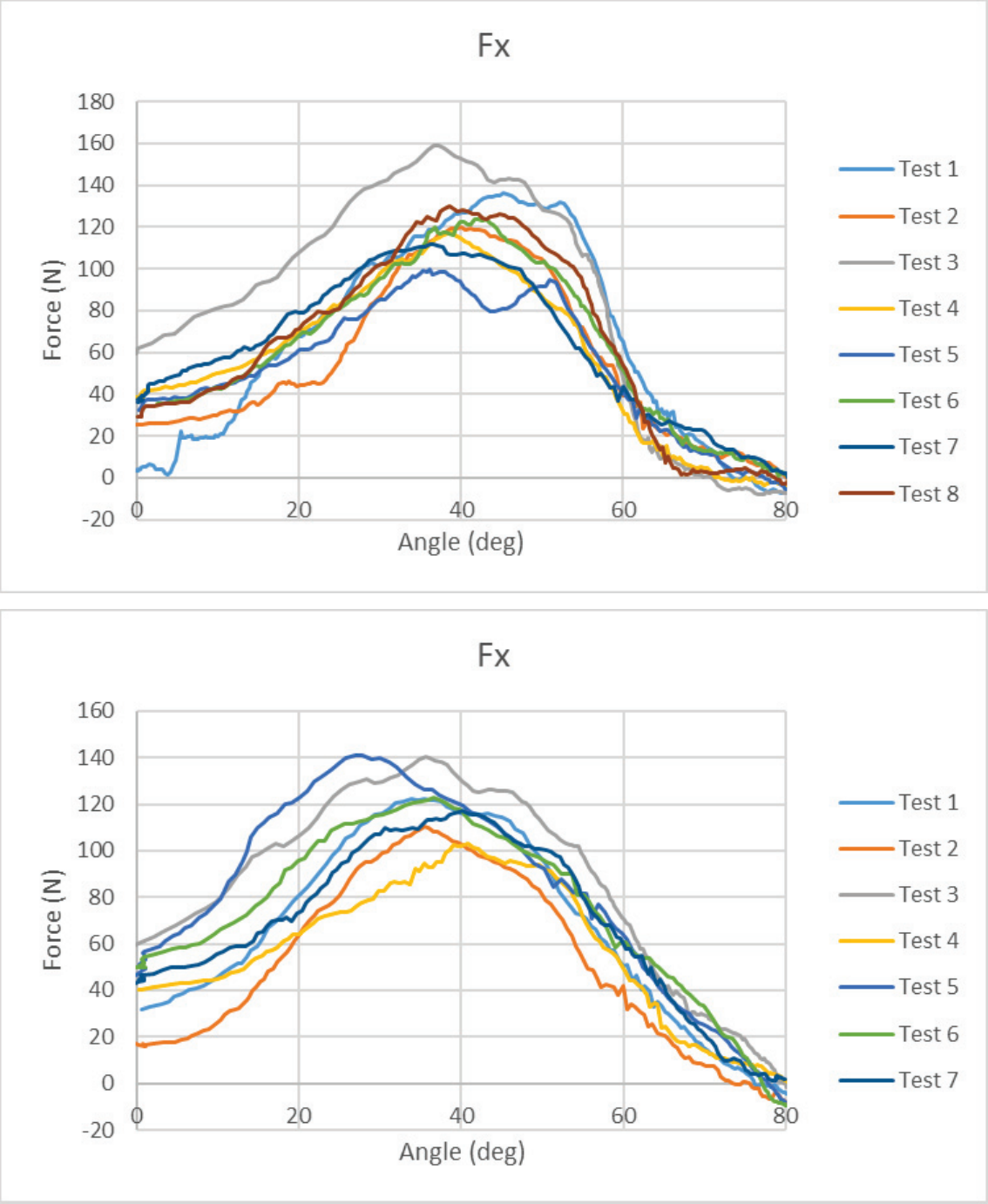

Figure 4.14. Required Actuation Force for Closing the Mechanism Without The Lower Window (Existing and Modified Spring Position)

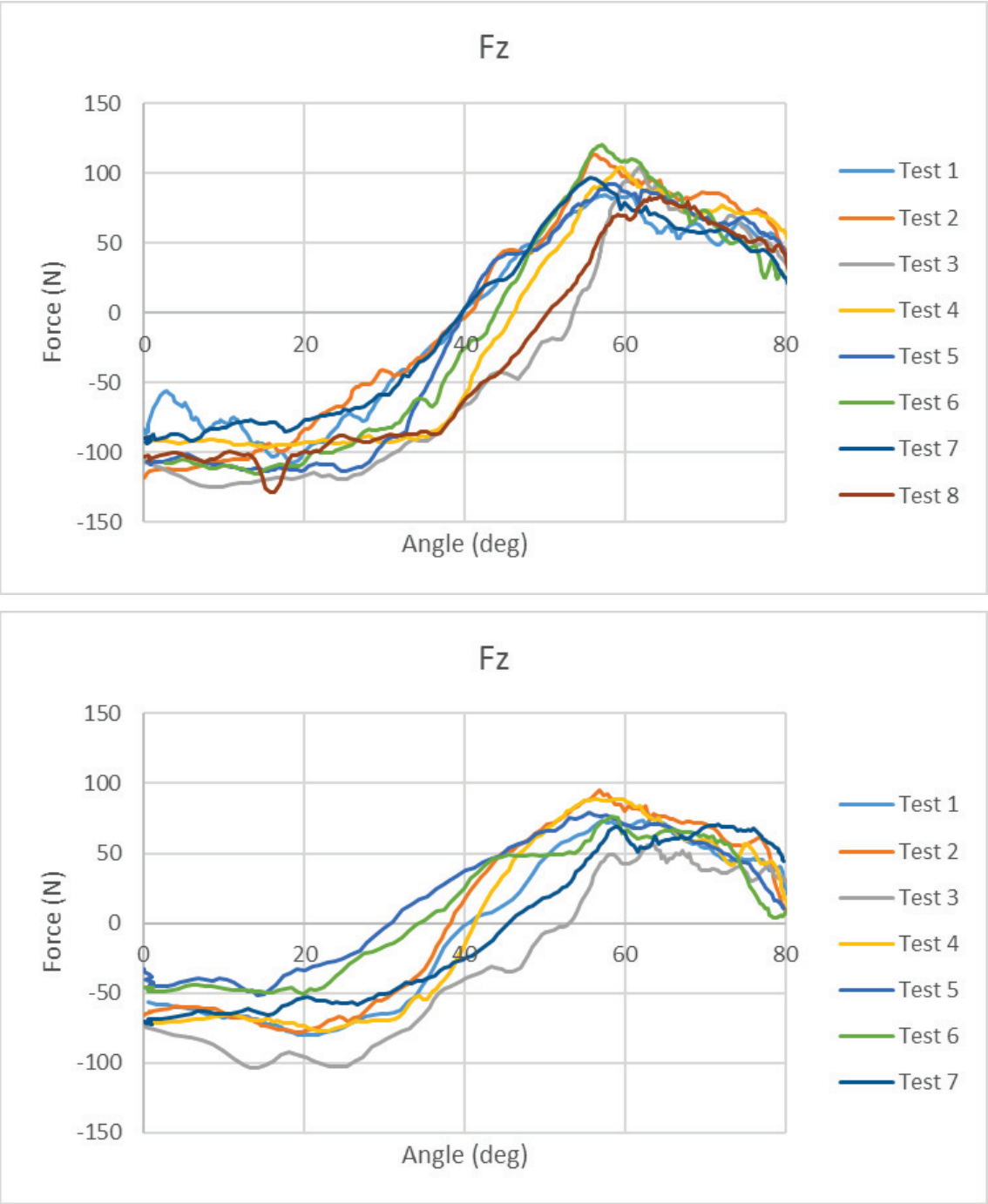

Figure 4.15. Required Actuation Force for Closing the Mechanism Without The Lower Window (Existing and Modified Spring Position)

The results in Figure 4.16 and Figure 4.17 are measured manual force components for opening the mechanism with the lower window attached. In this configuration of the mechanism the opening is the critical motion rather than closing due to the increase in weight of the window. As it can be seen from Table 4.1 with the new

spring position there is a decrease in the required actuation force in z-axes which is the critical one.

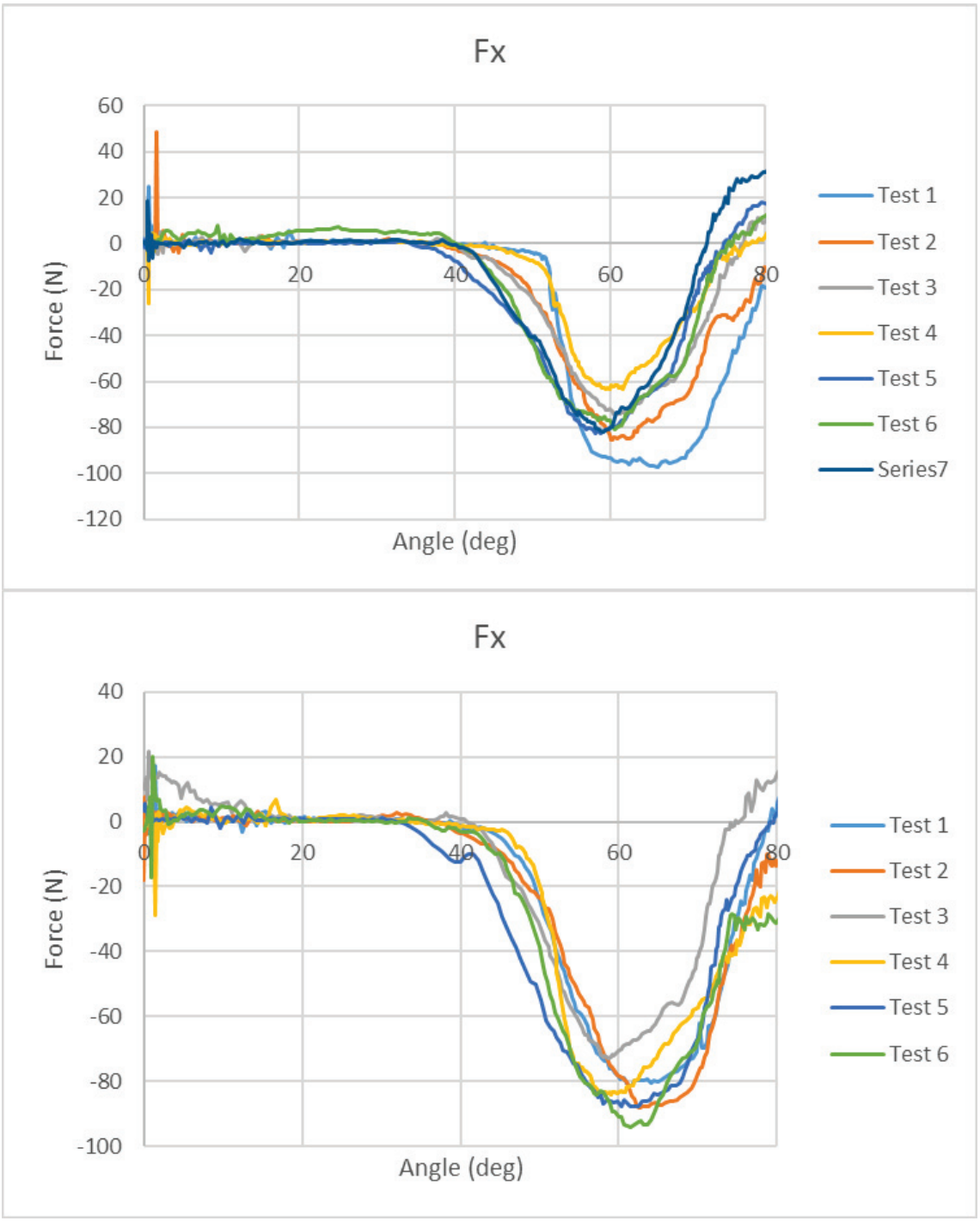

Figure 4.16. Required Actuation Force for Opening the Mechanism With The Lower Window (Existing and Modified Spring Position)

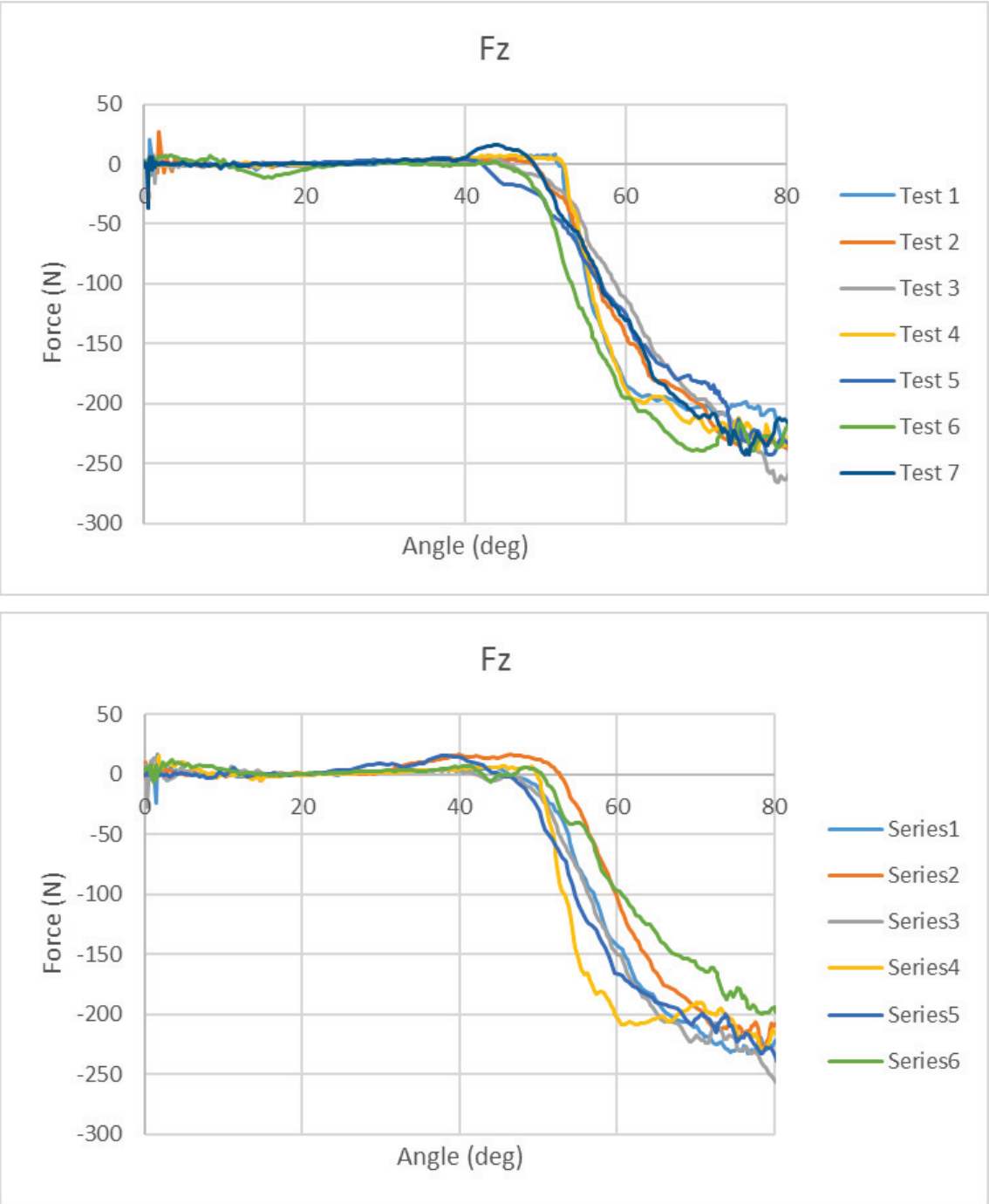

Figure 4.17. Required Actuation Force for Opening the Mechanism With The Lower Window (Existing and Modified Spring Position)

The results in Figure 4.18 and Figure 4.19 are manual force components for closing the mechanism with the lower window attached. During this motion the increased weight of the mechanism decreases the force requirements with respect to the configuration without the lower window hence this direction of motion is not critical.

From Table 4-1 it can be seen that the closing force requirement is reduced in the modified location of the spring.

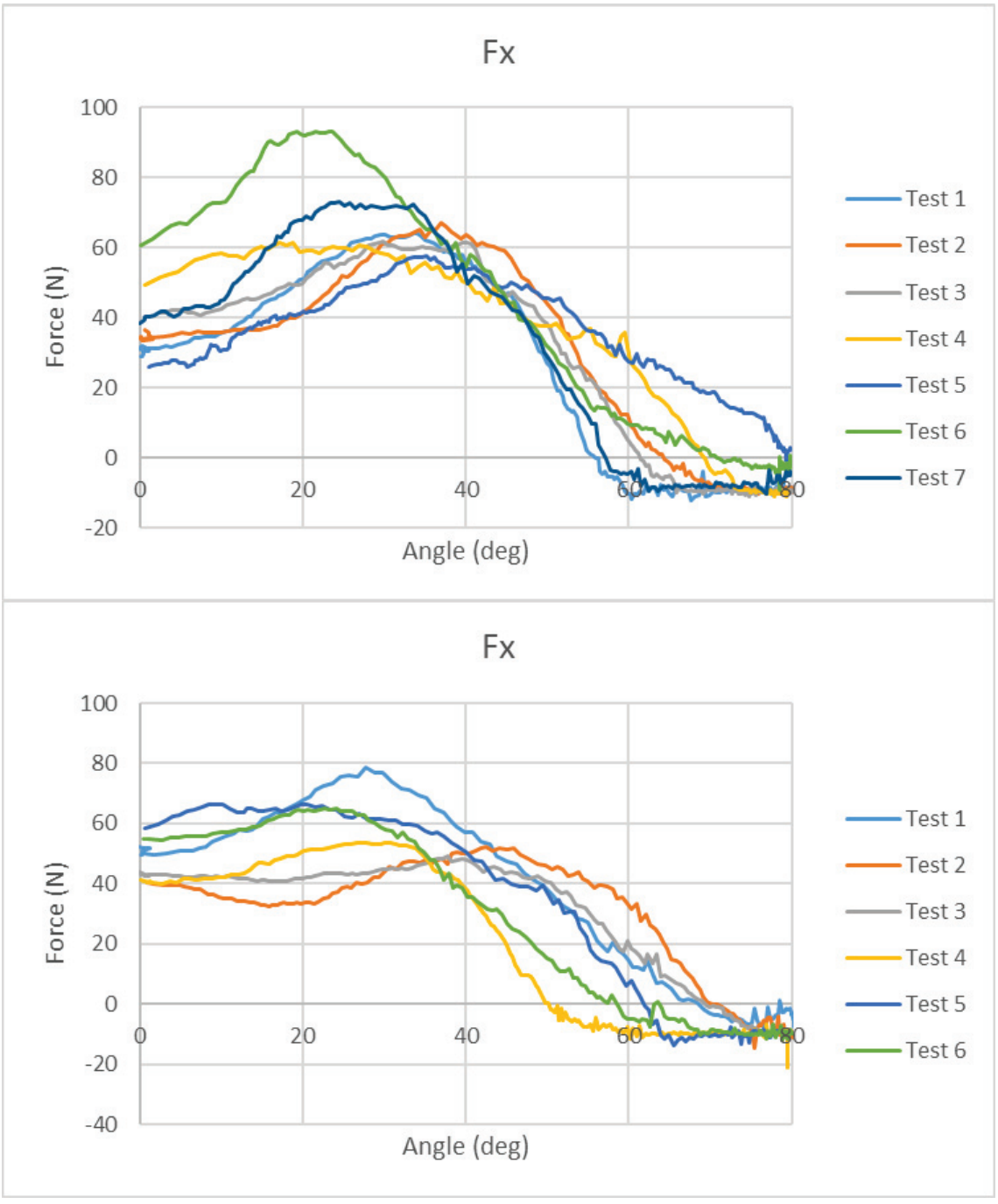

Figure 4.18. Required Actuation Force for Closing the Mechanism With The Lower Window (Existing and Modified Spring Position)

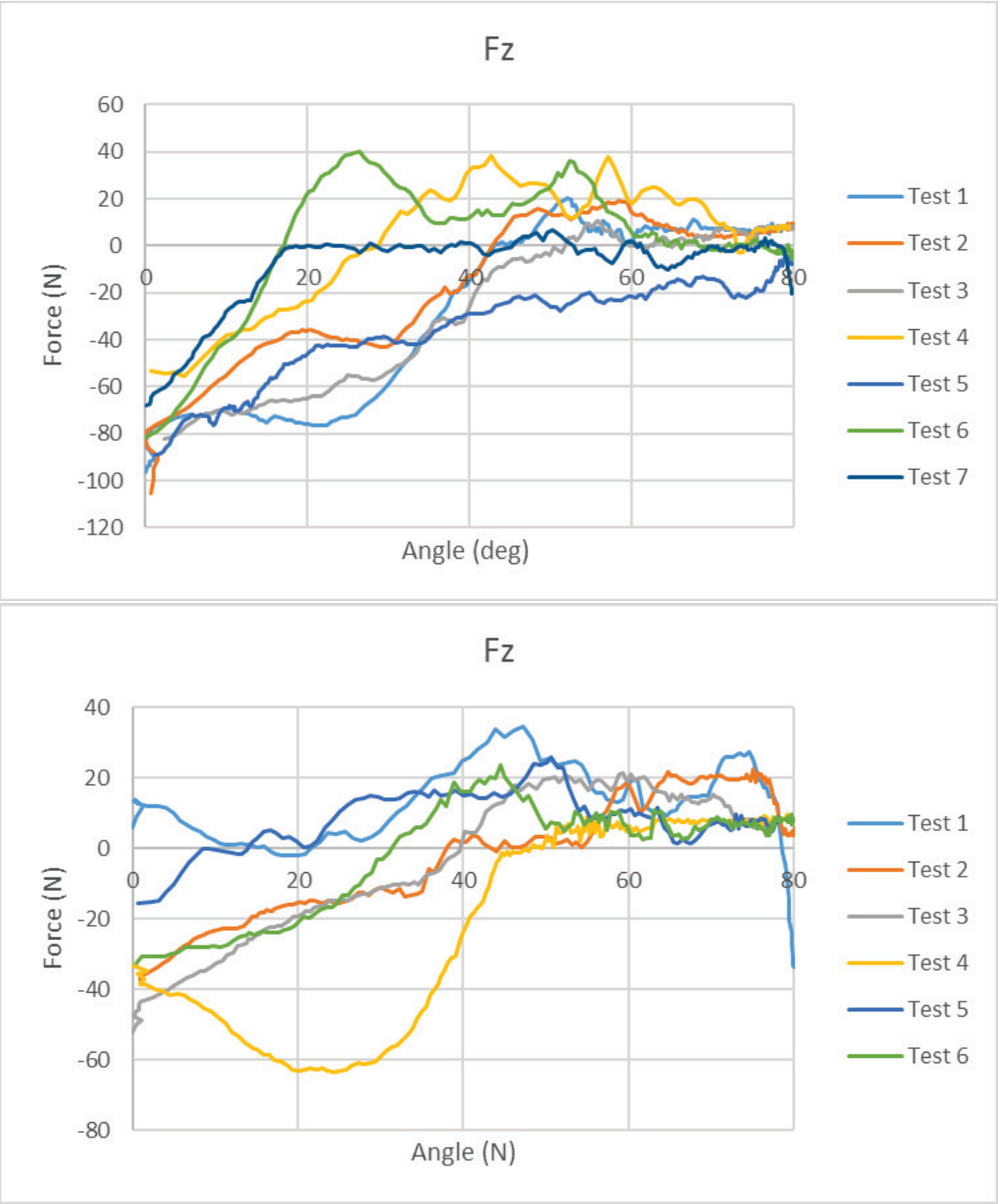

Figure 4.19. Required Actuation Force for Closing the Mechanism With The Lower Window (Existing and Modified Spring Position)

CHAPTER 5

DISCUSSION AND CONCLUSION

In this thesis the actuation force requirements of a window opening mechanism of an earthmoving machine is investigated. The aim is to minimize the required force that the operator needs to manipulate the mechanism. First the mechanism is analyzed in order to calculate for the handle force required to actuate the existing mechanism. The mechanism has two configurations, lower window attached or not, which results in different peak forces. With lower window attached, peak force is calculated as about 58.3 N during opening and 96.7 N during closing. Without the lower window attached the peak force is estimated 128.1 N during closing and there is no significant force requirement during opening.

The first solution sought for decreasing the maximum force requirements was optimization of spring position, to be more specific, optimizing the attachment point of the spring with the chassis whereas the spring characteristics remain the same. With the lower window attached, the estimated peak force slightly increased to 62.9 N during opening and reduced to 73.1 N during closing. Without the lower window attached, the peak force for closing is reduced to 109 N. The increase during opening is very small with respect to the reduction we have in the other directions.

In the link length optimization solution, there is no overall minimization of the force curve. As link lengths are changed, different portions of the curve improve, while the other portions get worse. Also changing the position of the handle did not decrease the maximum force requirement. These analyses of the mechanism and also the slight improvements with the spring position modification indicates that the original mechanism and the spring location is already well optimized and just some fine tuning may be utilized.

The results of the spring position optimization were tested with a simple test setup. In the configuration without the lower window there are no improvements in the critical points. In the configuration with the lower window during opening there is an improvement of about 15 N for the peak force, whereas in closing there is an improvement of about 7.5 N. Also the results show that the work done by the operator is reduced with

the modified spring position in all configurations and directions of motion except opening without the lower window case, which is not critical.

As future works a new mechanism may be sought in order to decrease the required actuation forces, taking into account several constraints such as the shape of the cabin and the window profile.

REFERENCES

Mecalac.”MCR Mecalac”. Mecalac.com
http://www.mecalac.com/files/bibliotheques/1479468380_6-8-10mcr-mk327-gb-10-16-pdf.pdf
(accessed July 23. 2017)

Takeshi Hiraoka, Yoshihiro Nagata, Kazuhiro Suzuki, Mikiya Yagi, Shigemasa Yamashita and Mitsukane Yazawa. Front Window Opening/Closing Device of Cabin for Construction Machine. JP Patent JPH04208632 filed November 29, 1990 and issued July 30, 1992.

Tokuo Fujii and Hideku Ookubo. Construction Machine. US Patent 20070108796 filed September 29, 2006, and issued May 17, 2007.

Takeshi Kakegawa and Tatsuhiro Murakami. Windshield Opening/Closing Device of Construction Machine. JP Patent JP2009249811 filed April 1, 2008 and issued October 29, 2009.

Toshiya Hayashida and Tomoya Hirano. Window Structure for Construction Machine Cab. JP Patent 2014213674 filed April 24, 2013, and issued November 17, 2014.

Eres Soylemez. Mechanisms. (Ankara: METU, 2009)

Stabilus GmbH. “Gas Springs and Dampers for Industrial Applications”. Stabilus.com. http://www.stabilus.com/fileadmin/download/Stabilus_Industrie_12_05_engl.pdf. (accessed July 23. 2017)